INVESTIGATION OF WATER GAS SHIFT REACTION OVER MOF ASSISTED PRECIOUS METAL CATALYSTS

by

Hayri Onur Kavaklı

B.S., Chemical Engineering, Boğaziçi University

Submitted to the Institute for Graduate Studies in
Science and Engineering in partial fulfillment of
the requirements for the degree of
Master of Science

Graduate Program in Graduate Program in Chemical Engineering

Boğaziçi University

2014

ACKNOWLEDGEMENTS

First of all, I would like to express my gratitude towards my thesis supervisor Assoc. Prof. Ahmet Kerim Avcı for his insightful commentary and help over the past three years. His dedication towards his students and their work is essential, and is also what made this thesis possible.

I also would like to thank my thesis committee members, Prof. Ramazan Yıldırım and Assist. Prof. Alper Uzun for devoting their valuable time to read and comment on my thesis.

I would like to thank İrem Şen for holding my hand when I was just an inexperienced graduate and teaching the ropes about the system used in the presented work. Her devotion towards her friends and colleagues is inspiring, and I wish her the best in her current studies. I would also like to thank Mustafa Karakaya for his valuable commentary.

I would like to thank Özge Ertem for being there when I had fallen the most. Whatever happens, I will never forget your devotion and care towards me. It is not easy to find great people to friend, but I believe I have found an amazing one.

I also want to thank the departmental support staff Yakup Bal, Bilgi Dedeoğlu, Melike Gürbüz, Belgin Balkan and Başak Ünen for their help throughout these three years.

I would like to thank my closest friends Alper Ünsal and Yiğit Dikici for all the times we laughed and were serious, for every memory we had together. You guys deserve great things, and I am sure someday I will see you achieve them.

I would like to thank Berker Koççaz and Umut Soysal for opening their house to me whenever I needed. You can be sure I'll do the same for you.

My heartfelt thanks goes towards my friends in KB404, namely Can Ekici, Çiğdem Ekmen, Didem Büşra Kabakçı and Sinan Koç for making it easier in this hard path, I hope that your studies go well. Ring me up if you ever need any advice. Sincerely, your lab "head".

I would like to thank the rest of the CATREL group for their support and friendliness throughout these hard times, especially Melek Selcen Başar, Özgür Yaşar Çağlar, Doğa Demirhan, Elif Erdinç, Serhat Erşahin, Burcu Karagöz and İpek Paksoy.

I would like to thank Funda İdil Tezcan for the memories.

I would finally like to thank my family for supporting me unconditionally and lovingly throughout my life. I really am lucky to have such parents and a brother.

Financial support for this work is provided by TÜBİTAK through project 113M229.

ABSTRACT

INVESTIGATION OF WATER GAS SHIFT REACTION OVER MOF ASSISTED PRECIOUS METAL CATALYSTS

Low temperature Water-Gas Shift (WGS) reaction is investigated over MOF-supported Pt/MIL-53(Al) catalysts in 250-300 °C range and steam-to-carbon (S/C) ratios of 1.67, 2.33 and 3. Pt metal loadings of 0.5, 1.0 and 1.5 per cent by weight are compared. Apart from using it as a support, MIL-53(Al) is physically coupled to a well-known WGS catalyst, 1.5wt.%$Pt/CeO_x/Al_2O_3$, for the purpose of understanding the impact of using a MOF structure on WGS behaviour. The catalysts are prepared by the incipient-to-wetness impregnation technique using deionized water as the solvent. Highest CO conversion over the MOF-supported catalyst is found to be 72% at 300 °C and at S/C=2.33. Increase in S/C ratio and temperature are found to affect WGS activity, i.e. CO conversion significantly, while increase in Pt loading led to marginal elevations in activity. It is observed that the addition of MIL-53(Al) as either a support or alone increases CO consumption significantly, but this does not carry over to H_2 production. Extra tests show that steam addition over MIL-53(Al) is the primary cause of CO disappearance. H_2 is not affected by the mechanism that causes CO to decrease over MIL-53(Al). Single MIL-53(Al), single 1.5wt.%$Pt/CeO_x/Al_2O_3$ and their combination are tested. It is found that combined configuration has the highest CO conversion of 64% at 300 °C and S/C=2.33. MIL-53(Al) is found to be inert under the reaction conditions studied. SEM comparison of fresh and spent Pt/MIL-53(Al) shows that sintering occured throughout the reaction.

ÖZET

SU GAZI GEÇİŞ REAKSİYONUNUN MOF DESTEKLİ DEĞERLİ METAL KATALİZÖRLER ÜZERİNDE ARAŞTIRILMASI

Düşük sıcaklık su-gazı geçiş reaksiyonu MOF-destekli Pt/MIL-53(Al) katalizörler üzerinde, 250-300 °C sıcaklık aralığında ve S/C=1.67, 2.33 ve 3 değerlerinde araştırılmıştır. Yüzde 0.5, 1.0 ve 1.5 oranlarında Pt metal ağırlıkları karşılaştırılmıştır. Destek olarak kullanılmanın yanında, bir MOF yapısının WGS üzerinde etkisini anlayabilmek için MIL-53(Al) WGS reaksiyonunda iyi bilinen 1.5wt.%$Pt/CeO_x/Al_2O_3$ katalizörü ile fiziksel olarak birleştirilmiştir. Katalizörler ardışık emdirme yöntemi ile deionize su kullanılarak hazırlanmıştır. MOF-destekli katalizör üzerindeki en yüksek CO dönüşümüne %72 ile 300°C ve S/C=2.33'de ulaşılmıştır. S/C oranı ve sıcaklığın yükseltilmesi WGS aktivitesini, diğer bir deyişle CO dönüşümünü arttırırken, Pt ağırlığının etkisi marjinal bir seviyede kalmıştır. MIL-53(Al)'un destek ya da tek başına konmasının CO harcanmasını artırdığı, fakat H_2 üretimini etkilemediği gözlemlenmiştir. Ekstra testler buhar eklenmesinin CO harcanması üzerindeki ana etki olduğunu göstermiştir. H_2'in CO'in MIL-53(Al) üzerinde azalmasına sebep olan bu mekanizma tarafından etkilenmediğini bulunmuştur. Tek MIL-53(Al), tek 1.5wt.%$Pt/CeO_x/Al_2O_3$ ve bu ikisinin birleşimi test edilmiştir. En yüksek CO dönüşümü birleşik konfigürasyonda, 300 °C ve S/C=2.33 oranında, %64 olarak bulunmuştur. MIL-53(Al)'un reaksiyon koşulları altında inert olduğu saptanmıştır. Taze ve kullanılmış Pt/MIL-53(Al) arasında yapılan SEM karşılaştırması, reaksiyon sırasında sinterleme olduğu göstermiştir.

TABLE OF CONTENTS

LIST OF FIGURES

LIST OF TABLES

LIST OF SYMBOLS

C_{CO}^{in}	CO concentration in feed
C_{CO}^{out}	CO concentration in outlet
K_{eq}	Equilibrium constant
T	Temperature, (^oC)
X_{CO}	Carbon Monoxide conversion
ΔH^0	Standart Enthalpy of Reaction (kJ/mol)
σ	Vacant Active Site

LIST OF ACRONYMS/ABBREVIATIONS

ATR	Auto-Thermal Reforming
DUT	Dresden University of Technology
EDX	Energy Dispersive X-Ray Analysis
GC	Gas Chromatograph
HKUST	Hong Kong University of Science and Technology
HPLC	High Pressure Liquid Chromatography
ICE	Internal Combustion Engine
MFC	Mass Flow Controller
MOF	Metal-Organic Framework
MIL	Materials of Institut Lavoisier
PEMFC	Proton Exchange Membrane Fuel Cell
PROX	Preferential Oxidation
S/C	Steam-to-Carbon, molar
SEM	Scanning Electron Microscopy
TOS	Time on Stream
TCD	Thermal Conductivity Detector
WGS	Water-Gas Shift
XRD	X-Ray Diffraction
ZIF	Zeolitic Imidazolate Framework

1. INTRODUCTION

The dependency of day-to-day human life on the use of fossil foils, especially on crude oil, is unquestionable, whether it is producing energy, heating or transportation. However, the increasing scarcity of high quality crude oil and irreversible accumulation of pollutants such as CO_2 in the atmosphere upon fossil fuel consumption are two major challenges that need to be addressed. Alternative energy sources are constantly being researched. Although renewable energy sources like wind, hydro or solar energies have not reached high enough market shares to reduce the dependency on oil, this is expected to happen in the near future. In the meantime, more efficient and environmentally friendly methods of meeting the energy demand and of energy conversion technologies are being investigated.

One of the well-known methods is to use Proton Exchange Membrane Fuel Cells (PEMFC) either for supplying propulsion power in passenger vehicles or for supplying auxiliary power in larger size vehicles [1]. PEM fuel cells are known to operate at efficiencies higher than those of internal combustion engines, and do not involve any moving parts. These units, however, use almost pure hydrogen as the fuel. The most critical impurity is carbon monoxide (CO); even tens of ppm of it is sufficient to deactivate the fuel cell catalyst irreversibly [2]. Therefore, before being fed to the PEMFC, CO content of the feed gas should be reduced from a few per cents to less than 10 ppm [3]. This is where Water-Gas Shift (WGS) comes into play. The seemingly simple yet so complicated reaction is one of the most promising ways to reduce or balance the CO amount in a given stream.

The WGS unit is therefore considered as an integral part of the CO cleanup section fuel processing systems used to produce hydrogen both for mobile and stationary PEMFC applications. The use of WGS converters is not limited to fuel processing applications. They are traditionally employed to enrich the H_2 content of steam reformers used for producing pure hydrogen for important refinery applications such as

hydrocracking and hydrotreating.

Optimum sizing of the WGS units depends on the balance between kinetics and thermodynamics. Since the reaction is exothermic, H_2 production is favored at lower temperatures at which the reaction is kinetically controlled. The catalysts, which can be Pt or Au based in fuel processing applications, or Cu-based in refinery applications, become almost inactive below $\sim$ 200 ^{o}C [4]. Reactor design for operation at such temperatures will require higher catalyst loadings and bigger unit volumes. On the other hand, operation in above ca.300 ^{o}C, which is desirable in terms of catalytic activity and therefore possible with lower unit volumes, is limited by thermodynamics, and the reaction will shift in the direction of H_2 consumption. At this point, use of novel catalysts that can exhibit low temperature ($<$ 300 ^{o}C) catalytic activity can deliver CO conversions with less catalyst use and, therefore with smaller units operating with lower energy costs.

Metal-Organic Framework (MOF) materials have been the center of attention for about 20 years now. With hundreds of different MOF materials being researched and reported, the materials show much promise in heterogeneous catalysis, storage, separation, and substrate size selective catalysis due to their surface areas up to 5000 m^2/g accompanied by well-defined structures [5]. The materials vary in every aspect; from temperature stability to solvent stability, surface area to adsorption properties and so on. Finding high surface area MOF materials, which are suitable for use at moderate temperatures and with acceptable amounts of moisture resistance, is important for driving WGS. A MOF with these qualities could be used as a WGS support material in enhancing the reaction rates and decreasing the volume of WGS reactors. However, MOF-based catalysts have strict temperature limitations due to their organic content, and therefore require good temperature control.

The presented work includes low-temperature WGS reaction studied over MIL-53(Al) and 1.5wt.%$Pt/CeO_x/Al_2O_3$ using Pt as the active metal under a parametric plan. Variables tested include reaction temperature, feed gas composition and active

metal loading over the catalyst. In addition, XRD readings are presented for various solvents over tested MOF's, and catalyst surface imaging has been done by scanning electron microscopy (SEM) for fresh and spent catalysts.

The study contains 5 chapters. Chapter 2 consists of literature survey on hydrogen technologies, WGS reaction, MOF materials and the use of MOF's in catalysis. Chapter 3 includes the catalyst preparation techniques and reaction conditions studied. Results of the work and discussion is presented in Chapter 4. Chapter 5 involves major conclusions of the work and recommendations for future work.

2. LITERATURE SURVEY

2.1. Hydrogen Technology and Production

Conventional internal combustion engines (ICE) use fossil fuels to operate, which create strains on the environment and deplete the already dwindling fossil energy. The technology is going towards the use of fuel cells in automotive industry, which have much cleaner and sustainable operation conditions. The most highlighted fuel cell is PEMFC, which uses H_2 as its fuel source, due to its higher energy density which lowers the fuel cell in size compared to other fuel cells, low operating temperature at about 100 °C, up to 40000 hours of operation and quick start-up ability for transport applications. The biggest issues with this type of fuel cell is its low operating efficiency at 40-45% and the expensive platinum membrane which deactivates irreversibly when subjected to CO levels higher than 10 ppm [6].

With the increase of attention for PEMFC as a clean alternative to reduce automotive pollution, H_2 has seen immense amounts of increase of research in production and transportation applications as PEMFC requires nearly-CO-free H_2 feed gas [3]. Many different feedstock for H_2 production are being researched, the ones with highest market share and promising future are listed below [7]:

- Coal
- Water
- Biomass
- Natural gas

Coal gasification processes have received interest due to the presence of vast deposits of coal. However, coal is a complex hydrocarbon which, upon gasification, gives a wide product distribution with low hydrogen purity. Moreover, high amounts of sulfur present in coal necessitates extra sulfur removal operations. Biomass, which is

a sustainable hydrocarbon source, can be used as a feedstock for producing ethanol, methanol, biodiesel or pyrolysis oil, which can be transported and converted to H_2. The problem associated with the use of biomass, however, is its required amount for a feasible H_2 economy, as there are other industries (e.g. food industry) that greatly benefit from the use of biomass. Water can be used for H_2 production through thermal splitting or electrolysis. Thermal splitting is being investigated for reducing the temperature of the process from 2000 °C to 450 °C using hydrogen iodide. The problem with this process is rapid recombination of H_2 and O_2 back to H_2O. Electrolysis is also under heavy development. Electricity cost directly affects H_2 cost in this process, possible ways to provide the energy are nuclear, geothermal or solar-based configurations. Electrolysis has its own bottlenecks, such as low efficiency and water purification to preserve electrolysis cells [7].

Today, most of the H_2 production is carried out by steam reforming of natural gas, which is composed mostly of methane: [8]:

$$CH_4 + H_2O \rightleftharpoons CO + 3H_2,\ \Delta H^0 = 206\ \text{kJ/mol} \tag{2.1}$$

This reaction is sometimes accompanied by partial oxidation (Reaction 2.2) or total oxidation (Reaction 2.3) to accommodate the energy requirement of steam reforming (Reaction 2.1). In such cases involving combination of oxidation and reforming, the process is called autothermal reforming (ATR):

$$CH_4 + \frac{1}{2}O_2 \rightleftharpoons CO + 2H_2,\ \Delta H^0 = -36\ \text{kJ/mol} \tag{2.2}$$

$$CH_4 + 2O_2 \rightleftharpoons CO_2 + 2H_2O,\ \Delta H^0 = -802\ \text{kJ/mol} \tag{2.3}$$

These reactions produce a mixture of CO and H_2, which is called syngas. Syngas is a medium which can be used as fuel, as feedstock for Fisher-Tropsch process to manufacture synthetic oil, or a crude H_2 stream in need of further purification. Purifi-

cation is usually done through water-gas shift (WGS) (Equation 2.6) and preferential oxidation of carbon monoxide (PROX), the latter which is usually accompanied by H_2 oxidation [8]:

$$CO + \frac{1}{2}O_2 \rightleftharpoons CO_2,\ \Delta H^0 = -283\ \text{kJ/mol} \tag{2.4}$$

$$H_2 + \frac{1}{2}O_2 \rightleftharpoons H_2O,\ \Delta H^0 = -242\ \text{kJ/mol} \tag{2.5}$$

2.2. Water Gas Shift Reaction

WGS has long been used as a method of balancing the H_2/CO ratio in reformer outlet streams for Fischer-Tropsch and methanol synthesis, or to remove CO from the stream to purify H_2 for ammonia synthesis [9]:

$$CO + H_2O \rightleftharpoons CO_2 + H_2,\ \Delta H^0 = -41.2\ \text{kJ/mol} \tag{2.6}$$

$$K_{eq} = \exp\left(\frac{4577.8}{T\,(K)} - 4.33\right) \tag{2.7}$$

WGS is a reversible reaction and the reverse reaction is dominant at higher temperatures due to mildly exothermic nature of the reaction. The thermodynamic limitation forces the reaction to be conducted at low temperatures, where the barrier of kinetic limitation comes into effect. Total pressure does not effect conversion as the reaction stoichiometry is 1:1 [10]. Conventional method of obtaining purified H_2 is by subjecting the syngas to a high-temperature WGS reactor, which decreases the CO percentage at least to 3-4 % by volume due to the thermodynamic limitation, followed by a low-temperature WGS reactor to decrease the CO percentage below 0.5 % where the kinetic limitation becomes less severe due to pre-processed stream. In order to decrease the CO amount below 10-50 ppm range as required in fuel processing applications to drive PEMFC's, a PROX reactor is employed [3]. The first step, high-temperature WGS reaction is typically above 350 °C. Iron-chromium compounds are used as cat-

alysts for this phase due to their low cost and good resistance against sulfur. It has been long established that the iron compound is the active catalyst, whereas chromium is usually a stabilizer for the material. At high temperatures different reaction mechanisms such as an adsorbed decomposition mechanism, a redox mechanism and an interaction mechanism are proposed [8]. Though precious metals have been studied for high-temperature WGS, they have been found to be less active than copper. The reduced CO concentration to 3-4% has to be lowered, hence a low-temperature WGS reactor is employed. The prospect of using WGS inside automotive applications has shifted the attention away from high-temperature WGS, as it adds mass and volume to an already constrained space. Research efforts are concentrated in the way of a single and effective low-temperature WGS reactor.

The industrial application of WGS at low temperatures is done with copper-zinc catalysts today. However, the catalyst has low stability at temperatures greater than 300 °C, and is pyrophoric if it contacts air [11]. They are also irreversibly deactivated if they come into contact with liquid water. It has been shown that these materials are strongly inhibited by CO_2 and H_2O already present in the reaction [12]. Due to these constraints, researchers have focused on finding new catalysts with enough stability and reactivity for fuel processing applications. The disadvantages listed for copper-based catalysts have been overcome using precious metals. Precious metals have higher thermal stability than Cu-Zn catalysts, can be deposited on monolith or microchannel walls and are resistant to deactivation when compared to conventional catalysts. Kinetic studies have shown apparent activation energies as low as 46 kJ/mol [8]. These activation energies are significantly lower than those reported for Cu-based catalysts (ca. 80 kJ/mol) [9]. In precious metal catalyst mechanisms, it has been shown that the reaction is zero order with respect to CO, which, therefore, does not change the rate of reaction due to its partial pressure.

2.3. Water Gas Shift Catalysis

The requirements of a good WGS catalyst for H_2 production in fuel processing applications are as follows [13]:

- Non-pyrophoric. Must be able to contact air and oxygen without being deactivated.
- Does not require pre-reduction. The start-up cycle for the fuel cell must be minimal, requiring the catalyst to rapidly adapt to operating conditions .
- Can withstand rapid heating and cooling cycles.
- Size and weight of the reactor, which is directly connected to catalyst activity, must be reasonable.
- Cost of catalyst should be reasonable.

These important criteria are readily met by using precious metals as active component in a catalyst. Most studied metals are palladium, rhodium, platinum and gold. One of the first extensive studies to investigate precious metal catalyzed WGS found the following relative turnover frequency values at 300 ^{o}C [14]: Ru (60), Pt (20), Pd (4), Rh (3), Ir (1). They also reported that Pt/Al_2O_3 surpassed Pt/SiO_2 activity tenfold.

Ceria, as a promoter or a support, has long been researched with precious metals due to elevated WGS reactivities when compared to commercial catalysts [15]. The main problem in using ceria as a support comes from stability issues, as the catalyst activity continously diminishes over time. The loss has been attributed to several reasons, such as carbon formation on ceria and loss of metal dispersion and sintering over time [15]. Constant deactivation curve over time, coupled with testing in unrealistic feed conditions and short run lengths resulted in some researchers calling precious metal WGS catalysts to be an unrealistic endeavour and arguing that base metal catalyst research would be more fruitful [2]. In contrast, addition of zirconia has been shown to increase thermal stability against sintering [16]. The activity increase of ceria infused catalysts have been attributed to ceria being oxidized in its dormant state, promoting

the redox reaction occuring on the catalyst surface:

$$CO + \sigma \rightarrow CO_{ad} \tag{2.8}$$

$$H_2O + Ce_2O_3 \rightarrow 2CeO_2 + H_2 \tag{2.9}$$

$$CO_{ad} + 2CeO_2 \rightarrow CO_2 + Ce_2O_3 + \sigma \tag{2.10}$$

It has been argued that the irreversible loss of oxygen storage in ceria due to high temperature calcinations was the reason for WGS activity loss in ceria infused catalysts [17]. Another argument was that the CO was the reason for deactivation due to loss of metal surface area [18]. A last argument stated that the over-reduction of ceria due to H_2 present in the feed was the culprit for deactivation [19].

Apart from using ceria, WGS activity can also be improved by the use of other promoters. Addition of TiO_2 on Pt/CeO_2 catalyst has been shown to increase thermal stability and decrease the temperature required to reduce the catalyst [20]. Adding Re on Pt/TiO_2 has been shown to increase activity significantly [21]. Also, addition of Fe_2O_3 on ceria supported Pd has been shown to increase activity tenfold [15]. These examples clearly show that promoter effects on precious metal catalysts are very important, and need to be considered before coming to a conclusion.

Comparative activity studies have been done for many different active metals and supports under realistic reformate conditionsn [22]. It has been shown that at 300 ^oC highest performing WGS catalyst was Pt/TiO_2, followed by $Pt/CeO_2 - Al_2O_3$ and Au/CeO_2. It has been also shown that Au catalysts had the lowest activation energy by a large margin, making them suitable for even lower temperature WGS research. It has been noted that H_2 and CO_2 have negative effects on the activity of WGS catalysts.

Comparative work has been done over ceria promoted Pt catalysts with different supports such as SiO_2, Al_2O_3, TiO_2, CeO_2 and $SiO_2 - Al_2O_3$ under harsh reformate

conditions [23]. The results show that $Pt-Ce/TiO_2$ catalyst performed with the highest activity with a turnover frequency of 0.63 s^{-1} and stability in start-up/shut-down operations even at low temperatures. It has been also emphasized that the catalyst synthesis method mattered and single-step co-impregnation was the most optimal technique.

It has been found that metal oxides supports play a great deal when WGS is in question. Irreducible supports such as Al_2O_3, MgO and SiO_2 have shown inferior activity in WGS, about 1-2 orders of magnitude, than reducible supports, such as TiO_2, CeO_2, and La_2O_3 when the active metal was Pt and Ru [24]. This behaviour was predicted by others before [17]. This leads to a regenerative mechanism where the CO adsorbed on the metal is oxidized by reducing the metal, which in turn is oxidized by water forming H_2. Between the reducible supports, TiO_2 has been shown to have superior performance over CeO_2. It has also been shown that the catalytic activity and turnover frequency of the catalysts did not depend on metal loading or dispersion of the active metal.

To further investigate support metal interaction in WGS, different research groups have worked on isolating the supports. Two different supports, namely $MgAl_2O_4$ and $Ce_{0.75}Zr_{0.25}O_2$ at 270 ^oC, have been investigated with a large number of active metals [25]. $MgAl_2O_4$ supported catalysts have been found to have activities in the decreasing order with respect to the dispersion of the metal in question: Cu>Pt>Rh>Pd>Re>Ni> Au>Ru$\sim$Co$\sim$Ag>Ir. Interestingly, $Ce_{0.75}Zr_{0.25}O_2$ supported catalysts were observed to follow the order of Pt>Re>Rh$\sim$Pd>Ru>Ni>Ir$\sim$Co>Cu>Ag>Fe>Au. The drastic change in some of the metals has been explained with the reactivity of the support itself. $MgAl_2O_4$ catalyst has been shown to perform best when the metal binding energy of oxygen was around -2.5 eV, whereas $Ce_{0.75}Zr_{0.25}O_2$ catalysts were shown to increase activity when CO adsorption strength of the metal increased. The difference is attributed to the redox mechanism on the $Ce_{0.75}Zr_{0.25}O_2$ support, whereas $MgAl_2O_4$ is inactive in the reaction. On a side note, $Ce_{0.75}Zr_{0.25}O_2$ supported catalysts have been shown to have higher activity values than $MgAl_2O_4$ supported catalysts, with the

exceptions of Cu and Au.

A study on promoter-support interface effect on the WGS reaction has shown that the catalyst activity increased when the catalyst was promoted with precious metals [26]. The effect was observed clearly when Cr_2O_3, U_3O_8 and $CeO_2 - ZrO_2$ were investigated. The authors attributed this effect of the precious metals to the acceleration of of merging and desorption of H_2 molecules and concluded that the support/catalyst, the promoter and the metal-support interactions affect the efficiency of WGS reaction.

Gold entered the catalysis scene when it was found out that the crucial point of the art was to finely disperse the gold particles in nano-sized chunks, in particular between $1 - 5$ nm [27]. After this, it has seen immense attention in low-temperature WGS due to some important factors [16]:

- Its non-pyrophoric nature, an essential requirement in automotive applications.
- Requires no pretreatment, making it very efficient in start-up and shut-down cycles.
- High activity, even surpassing that of Pt-Ce combined catalysts.
- Low activation energy, which in turn makes the WGS reaction possible at temperatures as low as 160 ^{o}C.

The kinetic studies of WGS reaction are immense and diverse in the literature. This is mainly due to the many different mechanisms occuring because of metal-support-promoter interactions. Smith et al. [28] have reviewed a wide range of publications covering many of the kinetics formulated until 2010.

2.4. Metal-Organic Frameworks

Metal-Organic Frameworks (MOF), also known as Porous Coordination Polymers (PCP) have seen enormous increase in attention for the last decade. This excitement

is due to many different and diverse properties of the materials, but it can be said that the most important point is the almost endless opportunities for engineering the right material for the right job on a rational basis. Some mind-blowing properties of MOF's are as follows [29]:

- Porosity of these materials can reach up to 90% of free volume, creating very-low density stable structures.
- These materials can reach surface areas up to and beyond 6000 m^2/g while retaining their structure. There are immense differences in surface areas from material to material, as MOF-2, MOF-5 and MOF-177 have surface areas of 270 m^2/g, 2900 m^2/g and 4500 m^2/g, respectively [30].
- These materials consist of a metal linker and organic ligands. The extraordinary variability of combinations and additives make these materials adaptable to almost any need.

Due to these properties, MOF materials have been worked on in many different fields and applications. Some of these materials are researched in storage applications, such as H_2 or CH_4 storage, some are used for separation purposes, due to their uses as high-capacity adsorbents and shape-selective properties. The materials have also been reported to exhibit catalytic properties. The HKUST-1 is a shining example for Lewis acid catalysis, such as selective oxidation of alkenes. MIL-100 (Fe, Cr) have been reported to be active in Friedel-Crafts benzylation due to their Brønsted acid sites. Base catalysis has been observed by directly synthesizing the MOF to include amino-functionalized ligands in the material. Polymerization reactions have also been highlighted due to the mesoporous structures of MOF's, especially when coupled with shape-selectivity. Entioselective catalysis, usually used in drug industry, has been found to occur on MOF's due to their potential homochiral and photoluminescence properties. One research group even suggested the use of MOF materials as semiconductors [31]. Last but not least, conventional catalysis using MOF's as supports are being actively investigated [4]. As observed, these materials have been found to be active and selective for a large variety of mechanisms, ranging from acid-base reactions

to redox catalysis. Although it is stated that it is unlikely for MOF's to penetrate mature chemical processes as catalysts, they may play a gigantic role in the production of bulky, large, high value-added chemicals.

Research over pore radii has come up with interesting results. Depending not only on the metal or ligand used, but also on the metal-to-ligand ratio, solvent and the source of the balance anions for metal ions during constructions have been found to tweak the pore size of the molecules in certain ways. Large mesoporous (20-500 Å) structures have been constructed, who have an advantageous stance in host-guest interactions, which in turn is a driving factor in catalysis. Some materials have been found to have pore diameters larger than 500 Å, which puts them in mesoporous category. On the other hand, working to decrease the pore diameter, researchers constructed MOF's with pore diameters than 20 Å which results in strong interactions between pore walls and gas molecules and make these materials suitable for gas storage and gas separation [32].

Scientists have already capitalized on these qualities and many researchers are continuing to work on expanding these opportunities. One of the most prominent areas is H_2 and CH_4 storage applications through surface adsorption on MOF's. Current hydrogen storage technologies use pressurized or cryogenic tanks, chemisorption and physisorption. Among these, physisorption has the advantage of fast kinetics, fully reversibility and easy heat management. The downside is that physisorption does not occur at ambient temperatures in conventional materials due to the low bonding energies between pore-wall material and H_2 [32]. The optimum bonding energy of 15.1 kJ/mol has been suggested for ambient temperature and low pressure storage [33]. Theoretically, it has been stated that the MOF structure can be tuned to have bonding energies between 10-50 kJ/mol using transition metals [34]. Ni has already been proven to have a heat of adsorption of about 12.9 kJ/mol [35]. The H_2 adsorption enthalpy is still a problem to overcome if the materials are to be used at ambient temperatures. It has been reported that physisorption alone may not be adequate enough to exceed liquid nitrogen density (70.8 g/L) [32].

The link between surface area and H_2 adsorption capacity has been found, which is a huge plus for using MOF's in H_2 storage. The problem is pore size. As stated, the surface area of these materials can differ immensely, but increasing the surface area of a MOF is usually accompanied by an increase in pore size, which is detrimental to pore wall−gas interaction. This decreases the gas adsorption energy of the molecule, therefore an optimization for this issue is required. Another problem is moisture, as some MOF's researched for H_2 intake are not stable in contact with water vapor. Optimally, a material with large surface area and pore volume, stable metal−ligand bonds and open metal sites is required for a positive progress in the field. A very large database of findings on H_2 adsorption is available [36]. Other gases, such as CH_4 [37] and CO_2 [38] have been studied extensively in their own rights. Even sulfur removal from fossil fuels is being investigated [39].

Gas separation and selective adsorption are other strong suits of MOF materials due to their shape selectivities. This is achieved through adsorbate−surface interactions and size exclusion due to molecular sieving effect. High porosity and the ability to optimize pore structure play well with the prospect of selective adsorption. Many different works have been assembled into a single review for the readers convenience [40]. Membrane-based gas separation is also in the works with these materials [41]. This area under heavy development due to the need of environmentally friendly and cost-efficient separation technologies.

One of the most interesting fields connected to MOF's is catalysis. Due to their high surface areas, large porosities and large pore sizes which stems from their framework structures, they have been regarded as potential candidates as catalyst supports. This is in addition to being used as acid-base and entioselective catalysts themselves. The framework structure highly decreases the dead volume, which is usually inaccessible, of a MOF support [42]. As a result, a theoretical MOF catalyst may have a very high density of exposed active sites per volume. Some catalysts have already been produced and reviewed [4, 42].

Although the listed structural advantages and properties are great for using MOF's in catalysis, there are some downsides to MOF materials. The first point is the structural instability of most created MOF's. Some MOF's simply cannot exist without a guest solvent residing inside their pores, making them unsuitable for heterogeneous catalysis [4]. Another problem arises due to the organic nature of ligands used in MOF's, as they tend to destabilize much more due to increased temperature than conventional catalyst supports. One last problem is moisture, as the water content in a stream tends to destroy the organic ligand inside the MOF's [30]. These setbacks have been solved for some MOF's as explained.

Water adsorption characteristics have been worked on HKUST-1, ZIF-8, MIL-101, MIL-100(Fe) and DUT-1 [43]. It has been found that the MIL materials and ZIF-8 were stable under water, whereas HKUST-1 and DUT-4 turned out to be unstable. It is very important to note that researchers described the ZIF-8 as highly inert but hydrophobic.

Another study on water stability of MOF materials have been carried out by Low *et al.* [44]. MIL-110, MIL-101, MOF-74, MIL-53(Al) and ZIF-8 have proven to be stable up to 300 °C with at most 50% steam in the streams. These values are usually not exceeded when low-temperature WGS reaction is worked, making these MOF's eligible for the study. The study, however, is not focused on building the MOF supports from scratch, therefore commercially available MOF's were chosen as the forward step. Sigma-Aldrich produces MIL-53(Al) and ZIF-8 under the trademark names Basolite A100 and Basolite Z1200, so these materials were further investigated.

MIL-53(Al) characteristics have been worked on in the literature [45]. It has been found that the surface area of the material is 950 m^2/g, with a micropore volume of 0.32 cm^3/g. The thermal stability up to 400 °C, chemical stability towards water and several organic solvents have been shown [46]. An interesting flexibility of MIL-53(Al) has been discovered by several groups [47–49]. It has been proven that a breathing effect occurs inside MIL-53(Al) upon guest molecule adsorption over a wide range of

molecules. This has led to the research of stability over large pore and narrow pore configurations on MIL-53(Al).

Au deposition on MIL-53(Al) using organometallic compounds and a novel deposition method, solid grinding has been investigated [50]. It has been observed that Au nanoclusters in average were 1.5 nm sized, which is a very important parameter in Au catalysis. It has also been proven to be active in benzyl alcohol oxidation. By adding amine functionalized groups, Pd particles have been stabilized in the material, and it has been found that the catalyst is active in Suzuki-Miyaura cross-coupling reaction with high yield and turn-over numbers [46].

Thermal and chemical stability of ZIF-8 has been extensively studied [51]. It has been found that the material is stable at temperatures up to 550 °C, with a high surface area of 1947 m^2/g, a pore diameter of 11.6 Å and a pore volume of 0.66 cm^3/g. It has also been noted that the material is stable in boiling benzene, methanol, water and aqueous sodium hydroxide, making it possible to use various organic solvents without seriously changing the surface chemistry of ZIF-8.

Another work has been done with MOF-5 and IRMOF-1 as the support using chemical vapor deposition as the deposition method [52]. Fe, Pt, Pd, Au, Cu, Zn and Sn metals have been loaded onto the MOF supports with up to 30% loading values without changing the chemical properties and framework structure of the MOF's. Au on ZIF-8 has also been worked on through solid grinding method [53]. It has been shown that CO oxidation at 300 °C occurs on the active metal. It has also been noted that the gold nanoclusters did not aggregate or migrate on the surface after the reaction with the particle size staying in the median of 3.1-3.5 nm, proving the stability of Au/ZIF-8 catalyst.

3. EXPERIMENTAL WORK

3.1. Chemicals

All of the chemical used for catalyst preparation are summarized in Table 3.1.

Table 3.1. Chemicals used for catalyst synthesis.

Chemicals	**Specification**	**Source**	**Molecular weight**
MIL-53(Al)	$C_8H_5AlO_5$	Sigma-Aldrich	208.10
Tetraammineplatinum(II) nitrate	$[Pt(NH_3)_4](NO_3)_2$ 50.4wt%Pt	Sigma-Aldrich	387.22
Gamma alumina	$\gamma - Al_2O_3$	Alfa Aesar	101.96
Cerium(III) nitrate hexahydrate	$Ce(NO_3)_3.6H_2O$	Sigma-Aldrich	434.22

3.2. Gases and Liquids

The gases used in the experimental system are presented in Table 3.2. The liquids used in catalyst preparation and support integrity experiments is listed in Table 3.3.

Table 3.2. Specifications and applications of the gases used.

Gas	**Specification**	**Application**
Argon	99.999% (Linde)	GC carrier gas
Helium	99.999% (Linde)	GC carrier gas
Carbon monoxide	99.999% (Linde)	GC calibration
Hydrogen	99.9% (Linde)	GC calibration, reduction
Nitrogen	99.998% (Linde)	Inert

3.3. Experimental System

This work consists of two different sections.

Table 3.3. Specifications and applications of the liquids used.

Liquid	**Specification**	**Application**
Deionized Water	Conductivity <0.1 μm.cm^{-1}	Catalyst Synthesis Reactant

Catalyst preparation system: The catalysts used in the parametric study of presented work is prepared by incipient-to wetness impregnation method.

Reaction system: The various parameters tested for the catalysts are input accordingly to the mass controllers for gas feed flow rates, HPLC pump for water feed flow rate and furnace for temperature control of the catalyst bed. Sampling is done over two calibrated gas chromotographs to analyze the feed and flue gas streams.

3.3.1. Catalyst Preparation System

All catalysts are prepared using the impregnation system illustrated in Figure 3.1. The system uses a vacuum pump for evacuating the support, Buchner flask for containing the support, a Retsch UR1 ultrasonic mixer for constant mixing and a Masterflex peristaltic pump for controlled impregnation of active metal.

3.3.2. Catalyst Preparation and Pretreatment

The catalysts used are prepared by the incipient-to wetness impregnation method except 1.5wt.%Pt/CeO_x/Al_2O_3, which is prepared by sequential impregnation method. For the catalysts using MIL-53(Al) as their support, no support preparation is needed as the particle size is already adequate for catalyst usage at 32.50 μm. The support is first evacuated at 105 ^oC in vacuum furnace, and afterwards placed inside a Buchner flask which resides on a Retsch UR1 ultrasonic mixer providing constant vibration for 30 minutes under vacuum conditions with the help of a vacuum pump. The calculated amount of tetraamineplatinum(II) nitrate is added to 1.7 ml of deionized water per 1 gram of support. The solution is mixed until homogeneous mixture is achieved,

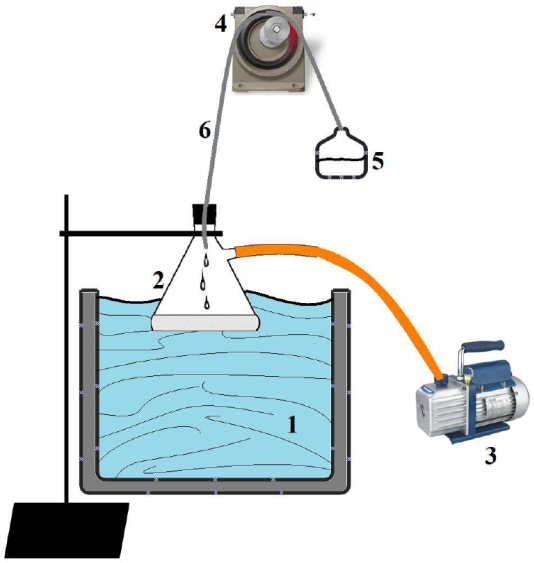

Figure 3.1. Schematic Representation of the Impregnation System. 1. Ultrasonic Mixer, 2. Buchner Flask, 3. Vacuum Pump, 4. Peristaltic Pump, 5. Aqueous Catalyst Solution, 6. Silicon Tubing (1.6 mm ID) [54].

and is impregnated to the support with the use of a Masterflex peristaltic pump at a flow rate of 0.5 ml/min. Making sure that the solution is spread equally over the support material, the catalyst slurry is left over the ultrasonic pump for 90 minutes to achieve uniform dispersion. Afterwards, the slurry is dried overnight for 16 hours in a furnace at 115 °C to evaporate the water used for impregnation. The dried catalyst is then calcined at 300 °C for 3 hours and stored in a dessicator until use. 1.5wt.%Pt/CeO_x/Al_2O_3 catalyst is prepared using this procedure twice, first for the impregnation of cerium and second for the impregnation of platinum atoms, hence it is named sequential impregnation method.

3.3.3. Catalytic Reaction System

The catalytic reaction and analysis system [54] consists of 3 subsections:

- Feed section
- Reaction section
- Product analysis section

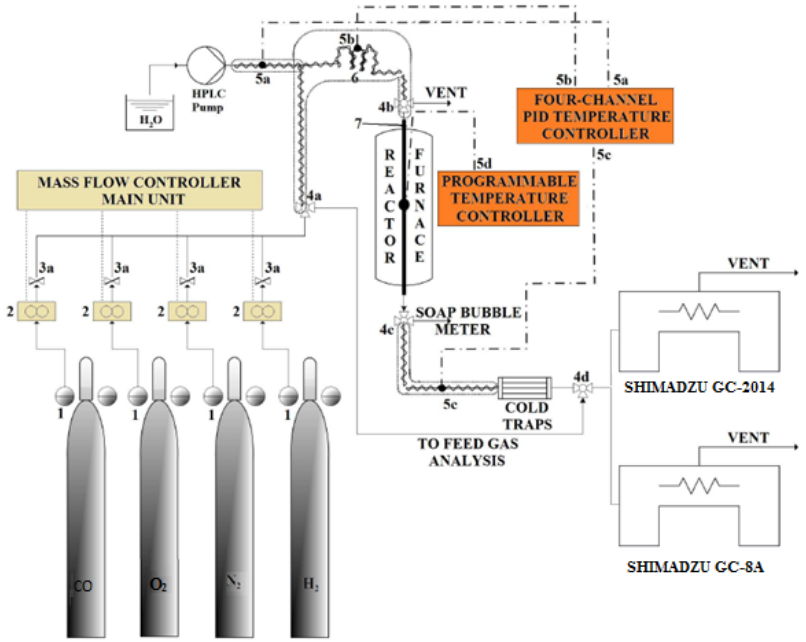

Figure 3.2. Schematic Representation of the Reaction System. 1. Gas Regulators, 2. Mass Flow Controllers, 3. On-Off Valves, 4. Three-Way Valves, 5. Thermocouple Locations, 6. Mixing Zone, 7. Quartz Tube [54]

3.3.3.1. Feed Section. The feed section contains purified N_2, H_2, CO and dry air for research purposes as outlined in Table 3.2, an Shimadzu LC-20AD HPLC pump for liquid pumping into the system, adequate tubing and fitting consisting of sizes 1/4", 1/8" and 1/16" from Swagelok for transportation of gases and liquid and mass flow controllers by Bronkhorst model F-201CV digital mass flow controller, whose calibration curves are provided in Appendix A.

The gas from the pressurized cylinders directly enter the flow controllers independently, and afterwards are merged for downstream. All lines are fit with open close valves to prevent back-pressure fluctuations and decrease the dead volume in the system when a line is not being used. The mass flow controller is used to determine the flow rate of individual gases, and to adjust the desired feed ratios. This stream is controlled by a three-way valve directing the flow toward either the reaction chamber or gas chromotographs for feed analysis. HPLC pump is used to pump the deionized

water into the system over 1/16" tubing without pulse formation. The liquid is then vaporized and kept at 120 °C before being mixed with the gas stream using heating tapes and K-type thermocouples with PID temperature controllers. The constant temperature of 120 °C is kept over the stainless stell tubing until the reactor chamber is reached. Just before entering the reactor, another three-way valve diverts the flow towards ventilation for 10 minutes, which is required for steady and well-mixed flow before the mixture reaches the catalyst.

3.3.3.2. Reaction Section. The reaction section of the system consists of a furnace which is controlled by a Shimaden FP23 Programmable Temperature Controller. A K-type sheathed thermocouple is used to control the temperature inside the reactor, which is connected to the FP23.

The feed gas enters the furnace which contains a 1/4" quartz tube serving as the reactor. The reactor contains the catalyst in the middle, which is placed at the center of the furnace with the thermocouple for minimum temperature fluctuation. After the gas passes through the reactor, it immediately enters an ice-cold water trap inside a Dewar flask, which separates the unreacted water from the effluent stream, and the rest of the products are sent over to the product analysis units.

3.3.3.3. Product Analysis Section. The product stream coming from the ice trap is directed to two different GC's with different configurations using a three-way valve. Shimadzu GC-2014 contains a Carboxen 1000 packed column with the ability to separate H_2, N_2, CO and CO_2 in high amounts. The other chromatograph Shimadzu GC-8A is fit with Porapak-Q column to further observe the CO_2 in the stream when it is at very low amounts, as this column can easily separate CO_2 from the other gases. Since it uses He as its carrier gas, it cannot differentiate H_2 from the other gases. Both GC's are equipped with thermal conductivity dedectors (TCD).

The chromatographs are calibrated for the gases in the product stream by injecting known amounts of the said gases inside the columns. The peaks obtained by this

method are correlated to the known volumes of the gases. These calibration curves are presented in Appendix B. The GC working conditions are summarized in Table 3.4.

Table 3.4. Shimadzu GC conditions for product analysis.

GC Parameter	**GC-2014**	**GC-8A**
Detector type	TCD	TCD
Column temperature	40 °C ($0 \rightarrow 13.5$ min) 40 →150 °C ($13.5 \rightarrow 15.5$ min) 150 °C ($15.5 \rightarrow 23.5$ min)	90 °C (10 min)
Injector temperature	110 °C	90 °C
Detector temperature	175 °C	150 °C
Detector current	50 μA	120 μA
Carrier gas	Ar	He
Carrier gas flow rate	30 ml.min^{-1}	25 ml.min^{-1}
Column packing material	Carboxen 1000	Porapack Q
Column tubing material	Stainless steel	Stainless steel
Column length & ID	6 m & 3 mm	1.5 m & 3 mm
Sampling loop	1 ml 25° C	1 ml 25° C

3.3.4. Catalyst Characterization Systems

Surface analysis of the catalyst samples were carried out by Boğaziçi University Advanced Technologies R&D Center through Backscattering Electron-Scanning Electron Microscopy (BSE-SEM) and Energy Dispersive X-ray Analysis (EDX) using a Philips XL30 ESEM-FEG unit, and through X-ray Diffraction (XRD) using a Rigaku D/MAX-Ultima and equipment.

3.4. Reaction Tests

To make sure that the construction and reactor material are inerts in WGS, blank tests were conducted under catalytic reaction conditions. No WGS activity was observed in quartz tubing and glass wool usage.

The reactor system can be observed in detail in Figure 3.3. Approximately 1 cm of glass wool is inserted in the system to prevent the catalyst from falling down the

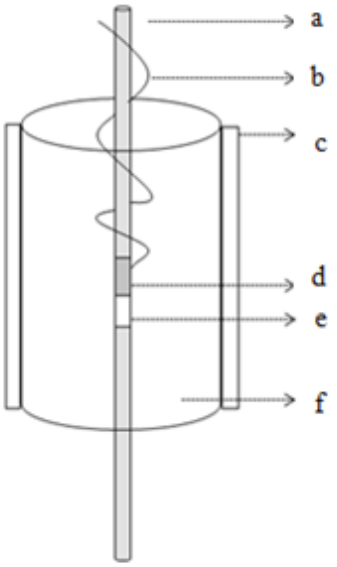

Figure 3.3. Schematic Diagram of the Packed Bed Reactor and Furnace System: a. Reactor b. Thermocouple c. Ceramic Wool Insulation d. Catalyst e. Glass Wool f. Furnace. [55]

reactor. A K-type thermocouple inserted next to the catalyst bed and attached to a programmable temperature controller that provides constant temperature monitoring and regulation.

The operating conditions used in the testing of WGS are summarized in Table 3.5. Parameters tested are temperature, active metal loading and S/C ratio. Flow rates are given in Table 3.6. The effect of fresh MIL-53(Al) over the reaction has been tested with 1.5%Pt/CeO_x/Al_2O_3. The experimental roadmap has been described in Tables 3.7 and 3.8.

Table 3.5. Operating conditions studied in WGS reaction.

Operating Parameters	**Parameter Values**
Reduction Temperature (°C)	300
Catalyst Amount (mg)	100
W/F Ratio (mg.min/ml)	1.43
Reaction Temperature (°C)	250, 300
H_2O/CO (ml/ml)	1.67, 2.33 , 3

Table 3.6. Feed conditions for WGS experiments.

CO (ml/min)	**H_2O (ml/min)**	**Total Flow Rate (ml/min)**
10	30	70
12	28	70
15	25	70

Experimental results have been reported in two different ways, the conversion of CO with respect to the feed, defined in Equation 3.1 and H_2 concentration in the effluent stream.

$$X_{CO} = 100 \times \frac{C_{CO}^{in} - C_{CO}^{out}}{C_{CO}^{in}} \tag{3.1}$$

Table 3.7. Experimental roadmap of Pt impregnated MIL-53(Al).

Catalyst	Temperature (°C)	S/C Ratio
1.5%Pt/MIL-53(Al)	250	1.67
		2.33
		3
	300	1.67
		2.33
		3
1.0%Pt/MIL-53(Al)	250	1.67
		2.33
		3
	300	1.67
		2.33
		3
0.5%Pt/MIL-53(Al)	250	1.67
		2.33
		3
	300	1.67
		2.33
		3

Table 3.8. Experimental roadmap of MIL-53(Al) and 1.5%Pt/CeO_x/Al_2O_3.

Catalyst	Temperature (°C)	S/C Ratio
MIL-53(Al)	250	1.67
		2.33
		3
	300	1.67
		2.33
		3
MIL-53(Al)+1.5%Pt/CeO_x/Al_2O_3	250	1.67
		2.33
		3
	300	1.67
		2.33
		3
1.5%Pt/CeO_x/Al_2O_3	250	1.67
		2.33
		3
	300	1.67
		2.33
		3

4. RESULTS AND DISCUSSION

The present work is divided into several sections. The first section consists of XRD results of MIL-53(Al) and ZIF-8 treated with several different solvents to find a suitable impregnation medium for the catalyst preparation. The second section contains the results of Pt impregnated MIL-53(Al) catalysts under various reaction conditions. The third section contains the results of physically coupled 1.5wt.%$Pt/CeO_x/Al_2O_3$ and MIL-53(Al) under different reaction conditions. The fourth section contains catalyst characterization results from SEM and EDX, over different fresh and spent catalysts. The fifth section contains some of the miscellaneous experiments done in order to obtain a deeper understanding of the catalytic process running over the configurations explained above.

4.1. XRD Results of ZIF-8 and MIL-53(Al) over Various Solvents

As stated, MOF materials are known to be susceptible to moisture and liquid water. This results in being a serious halt for catalyst preparation procedure, as deionized water is required in incipient-to-wetness impregnation method. In order to find out whether other organic solvents could be used during the impregnation, to obtain information over the deionized water's effect over tested MOF's and to see whether ZIF-8's hydrophobic nature would affect the use of incipient-to-wetness impregnation method, several XRD tests were conducted with certain parameters. The tested solvents; deionized water, acetone, hexane and methanol were all dripped on the MIL-53(Al) and ZIF-8 until all of the material was found to be barely wet, just as required in incipient-to-wetness method. The resulting solution was dried at 125 °C for three hours and afterwards sent for XRD. Untreated samples of MIL-53(Al) and ZIF-8 were also examined for the purpose of comparing the results.

4.1.1. MIL-53(Al)

MIL-53(Al) has already been tested under water vapour at different temperatures, and was found to be stable at 350 °C at 50% humid conditions [44]. However, this does not mean that the material will stay stable when in contact with liquid water. Figure 4.1 shows the resulting XRD of the untreated sample.

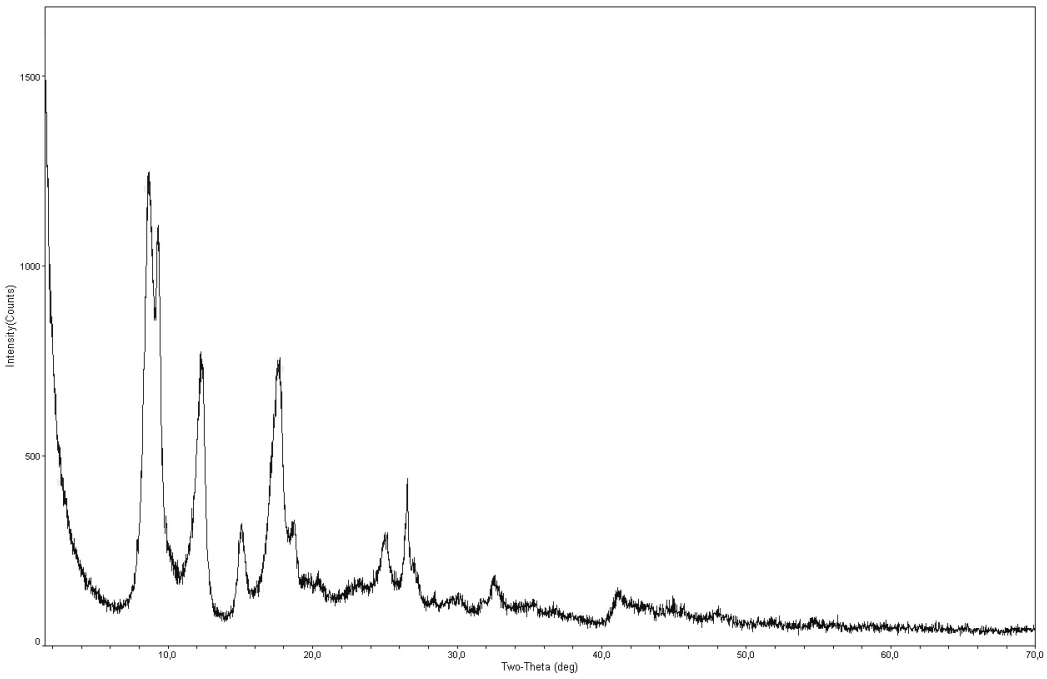

Figure 4.1. XRD Results for Untreated MIL-53(Al).

Figures 4.2, 4.3, 4.4, 4.5 and 4.6; which are solvent treated samples in the order of deionized water, IPA, acetone, hexane and methanol respectively; are individually compared to Figure 4.1 to find the changes in structure of MIL-53(Al), if any has occurred.

The effect of deionized water on the surface of MIL-53(Al) is somewhat diminished. Although no new peaks are observed between Figures 4.1 and 4.2, concluding that there are no new species formed on the surface, there are some peaks which lose their intensity slightly, at 10, 18 and 27 two-theta points. Other than that, there are no serious differences between the graphs, and it was concluded that water had min-

imal effect on the surface of MIL-53(Al). It has to be noted that when in contact

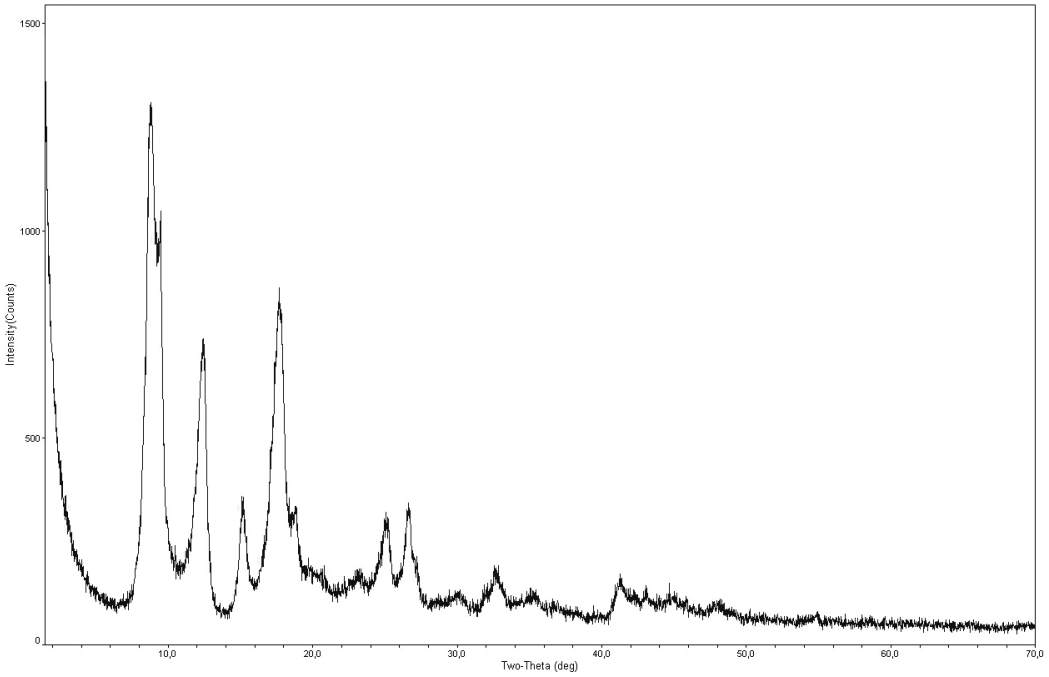

Figure 4.2. XRD Results for Deionized Water Treated MIL-53(Al).

with excess water, MIL-53(Al) showed signs of decomposition, such as intense bubble formation inside the muddy complex, and it was evident that the resulting slurry did not resemble the original MOF, instead the material solidified and multi-coloured spots were observed.

It has been observed that IPA showed results (Figure 4.3) similar to those of deionized water with the exception of two points. First, the 17 two-theta point seems to be intact under IPA and second, the region close to 45 two-theta has small but new peaks. The rest of the XRD result is identical to the deionized water case, with peaks at 10 and 28 two-theta's showing diminished intensity. While it may be plausible to use IPA as a solvent, the newly shaped surfaces are not good for such use.

The comparison of acetone treated and fresh MIL-53(Al) has shown that the solvent has detrimental effects over the structure of the MOF, as shown in Figure 4.4. The peak at 8 two-theta seems to rapidly increase, while surfaces defined in 12, 28 and

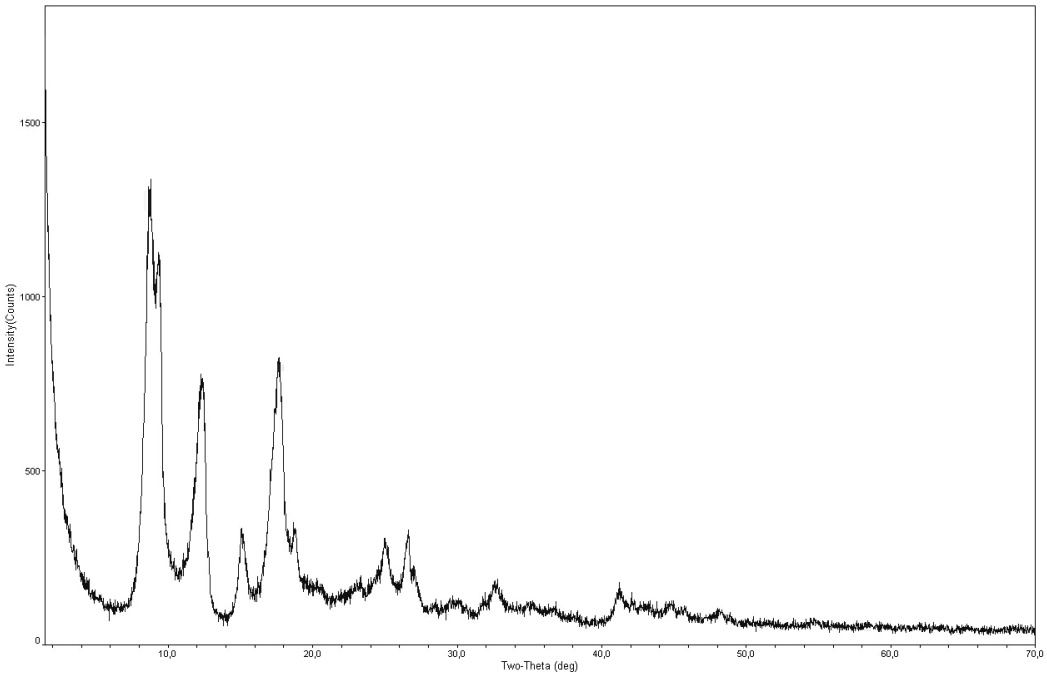

Figure 4.3. XRD Results for IPA Treated MIL-53(Al).

32 two-theta seem to diminish heavily or even disappear. It is clear that acetone is unsuitable for MIL-53(Al) impregnation purposes.

Hexane treatment in Figure 4.5 has shown similar results to acetone treatment, with the exception of 18 two-theta peak increasing in intensity. The rest of the surface seems to be affected in the same way as in acetone, marking hexane unfit for the role.

It is obvious in Figure 4.6 that methanol contact with the surface has massively altered the structure of MIL-53(Al). 8 two-theta peak is heavily diminished, while the peaks at 12, 18 and 27 are more intense when compared to a the untreated sample. The XRD results clearly show that methanol cannot be used as a solvent for MIL-53(Al).

Lastly, a qualitative analysis of untreated MIL-53(Al) can be observed in Figure 4.7. The components that matched in the database are not available in MIL-53(Al), such as zinc and phosphate, therefore the analysis was not taken into account.

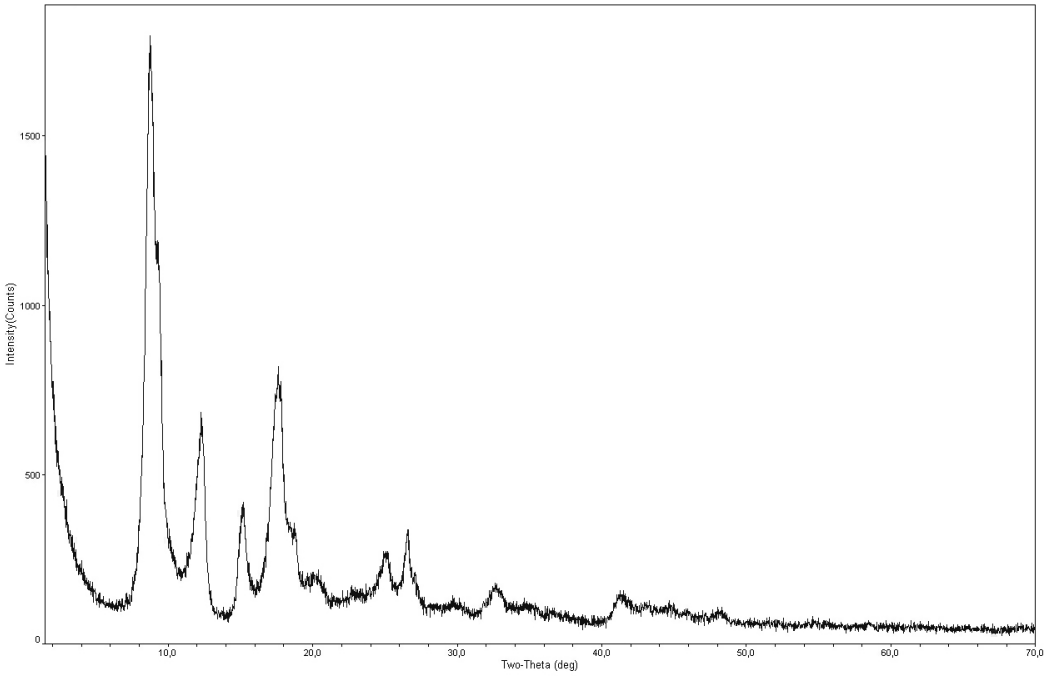

Figure 4.4. XRD Results for Acetone Treated MIL-53(Al).

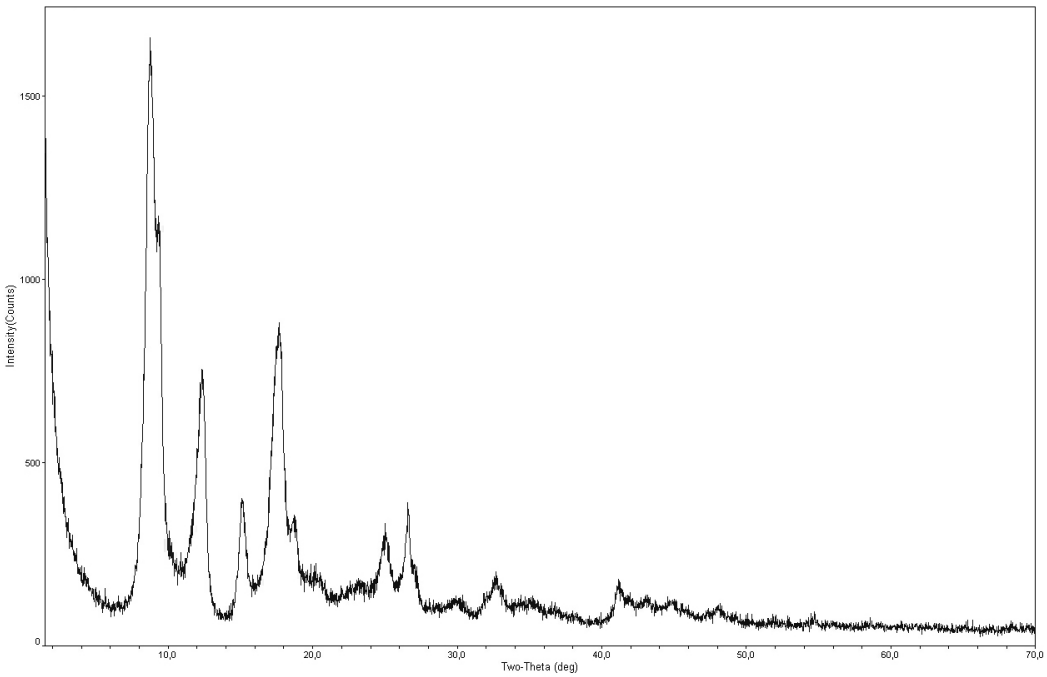

Figure 4.5. XRD Results for Hexane Treated MIL-53(Al).

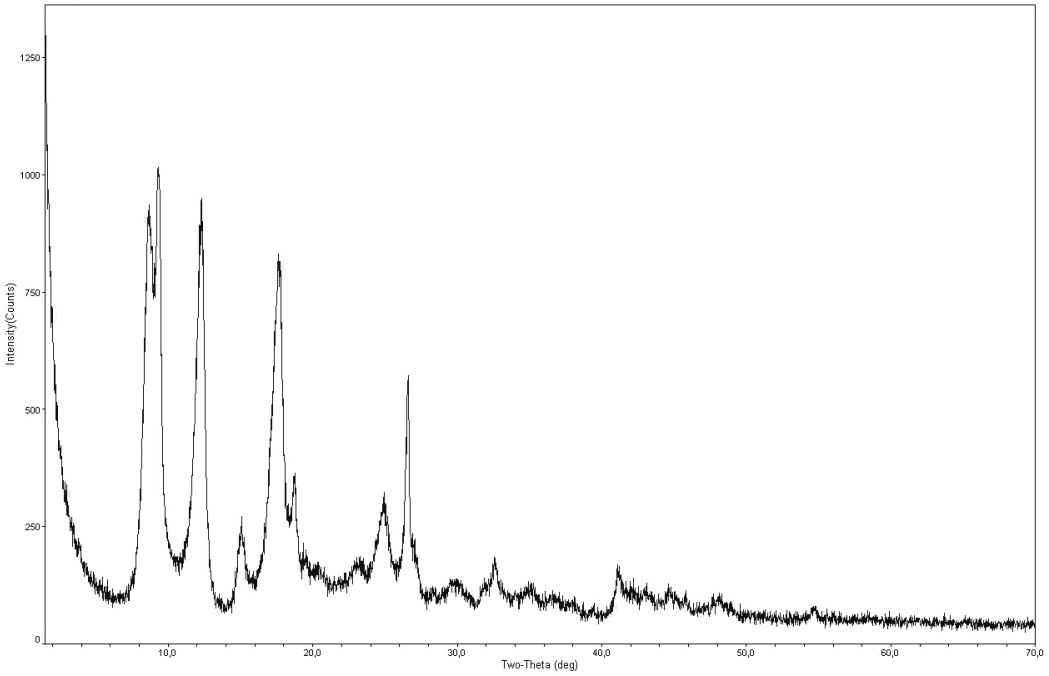

Figure 4.6. XRD Results for Methanol Treated MIL-53(Al).

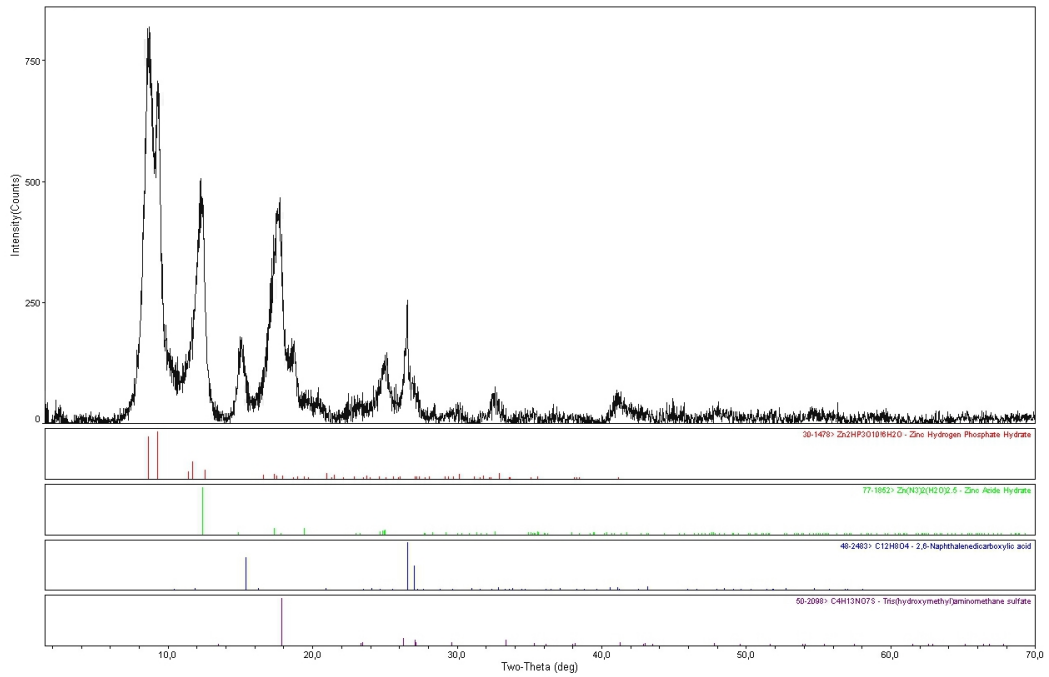

Figure 4.7. Qualitative XRD Results for MIL-53(Al) without Treatment.

4.1.2. ZIF-8

Due to their close resemblance to zeolites, ZIF family has gained fame in water resistance and temperature stability. The commercially produced member, ZIF-8 is subjected to the same conditions as MIL-53(Al). The XRD result of untreated ZIF-8 is presented in Figure 4.8.

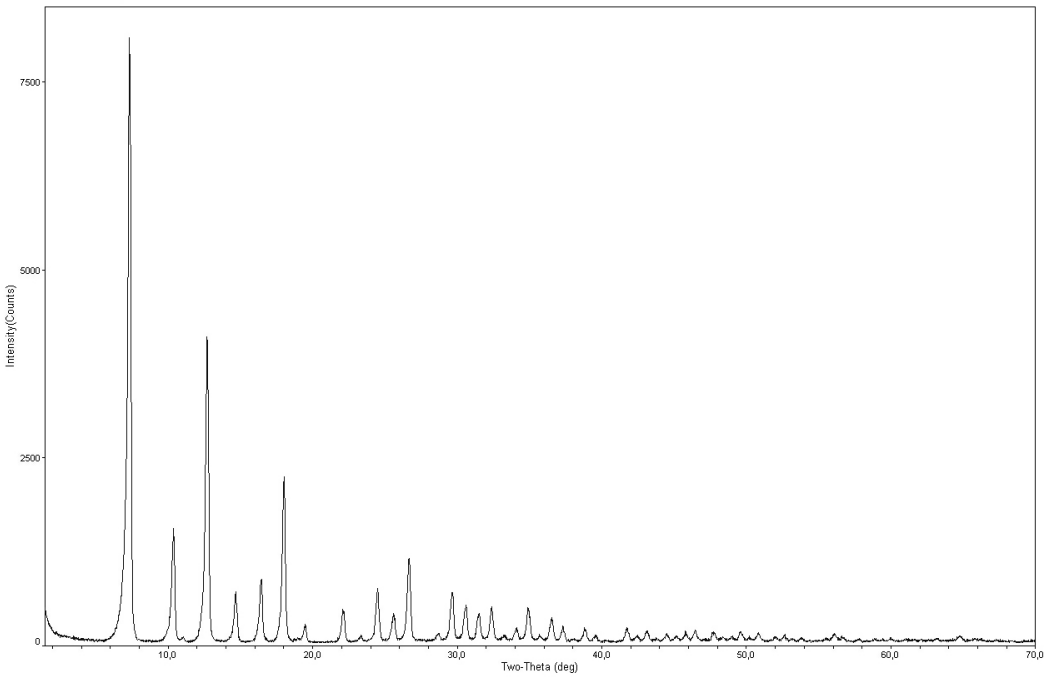

Figure 4.8. XRD Results for ZIF-8 without Treatment.

Figures 4.9, 4.10, 4.11, 4.12 and 4.13; which are solvent treated samples in the order of deionized water, IPA, acetone, hexane and methanol respectively; are individually compared to Figure 4.8 to find the changes in structure of ZIF-8. Lastly, a qualitative analysis of untreated ZIF-8 can be observed in Figure 4.14. The analysis makes sense, as the material complexes defined are plausible due to the content of ZIF-8.

ZIF-8 has proven to stay in stable form and keep its surface characteristics when in contact with IPA, acetone and hexane. Methanol greatly changed the surface complexes of ZIF-8, making it an unsuitable solvent for use. This result is different from what

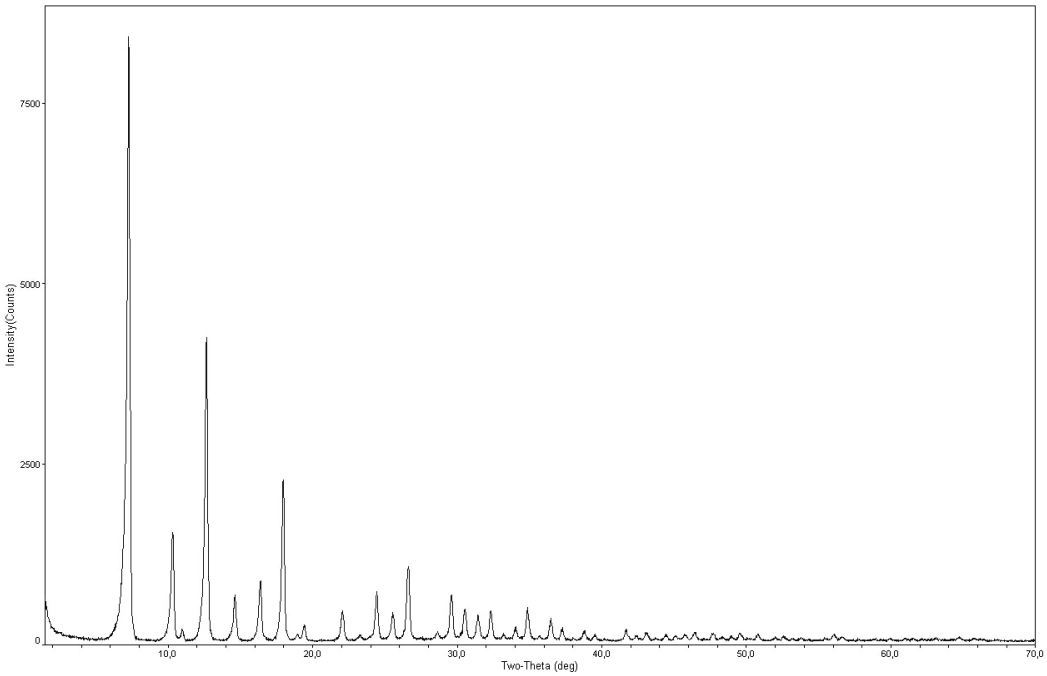

Figure 4.9. XRD Results for Deionized Water Treated ZIF-8.

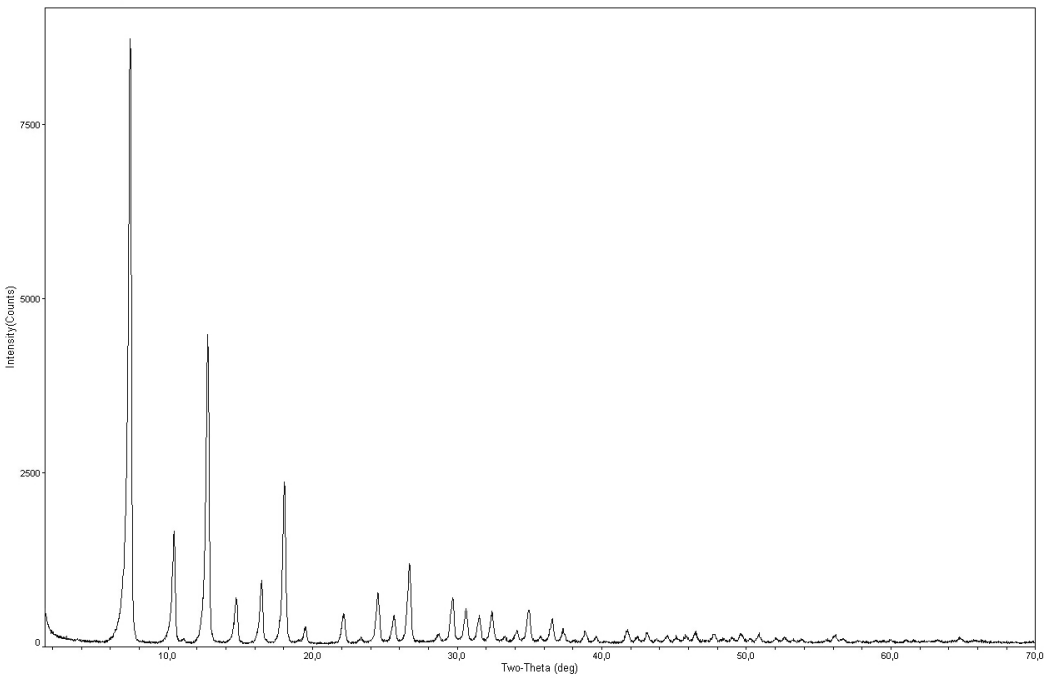

Figure 4.10. XRD Results for IPA Treated ZIF-8.

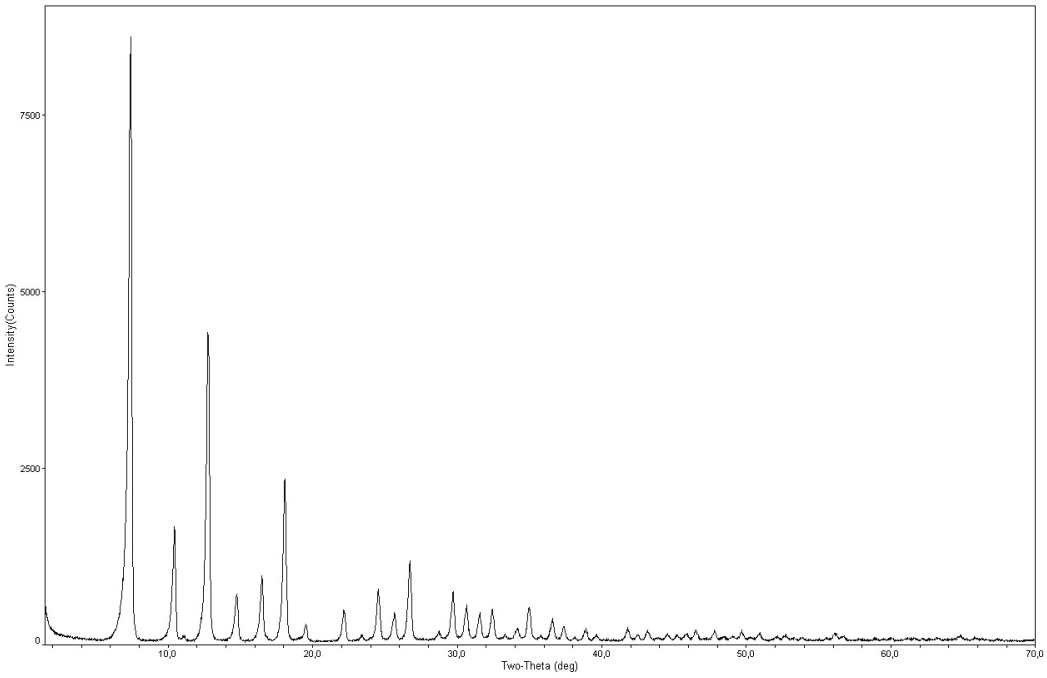

Figure 4.11. XRD Results for Acetone Treated ZIF-8.

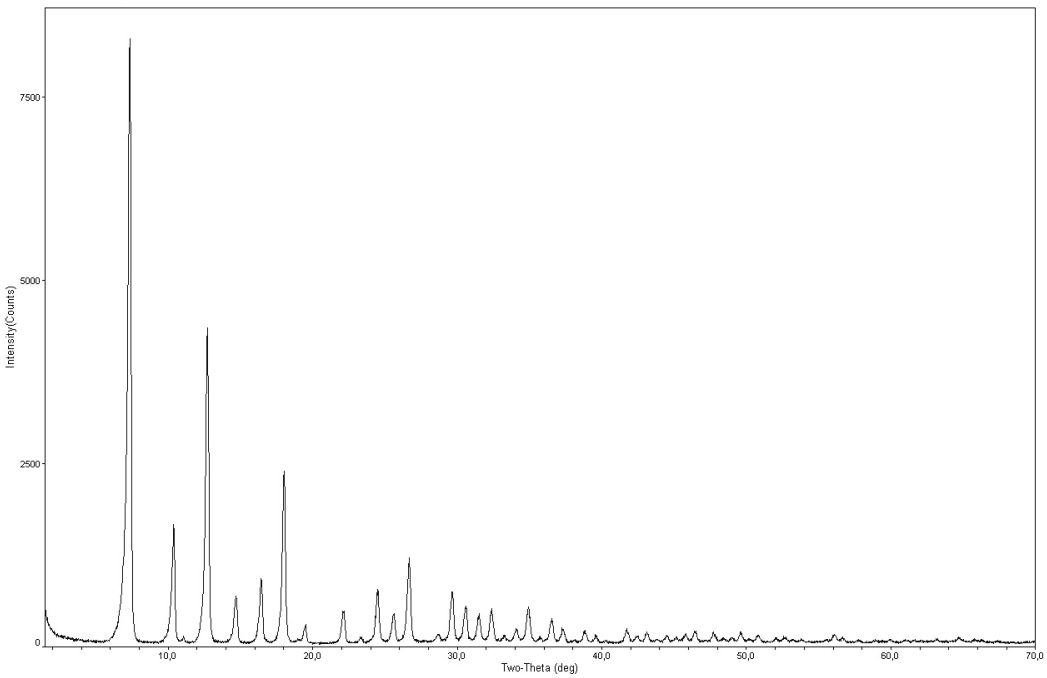

Figure 4.12. XRD Results for Hexane Treated ZIF-8.

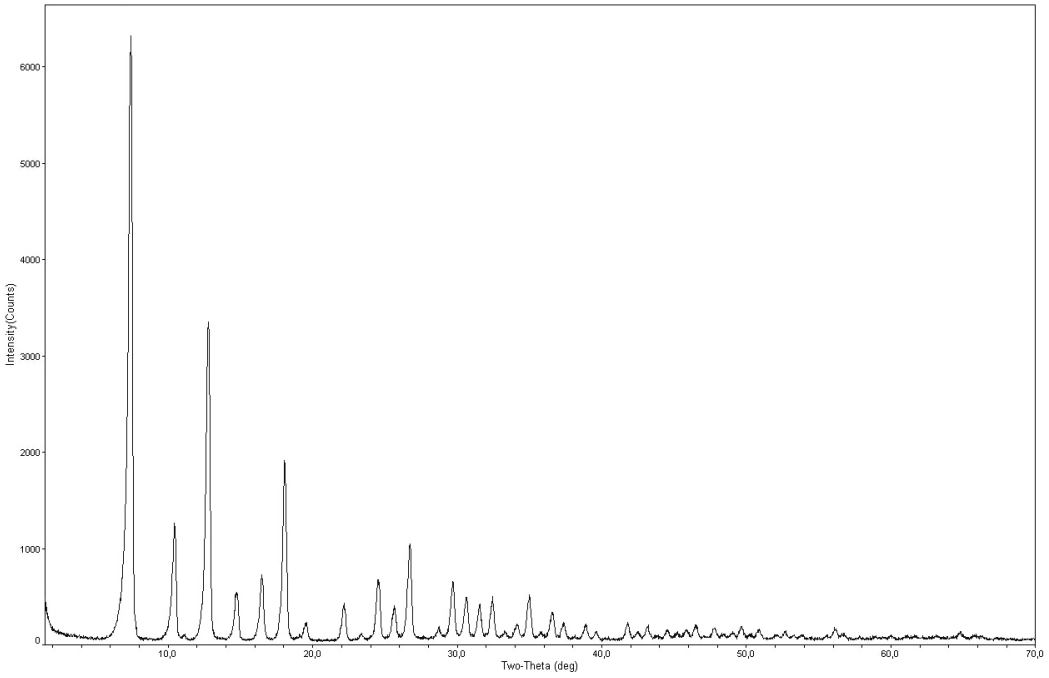

Figure 4.13. XRD Results for Methanol Treated MIL-53(Al).

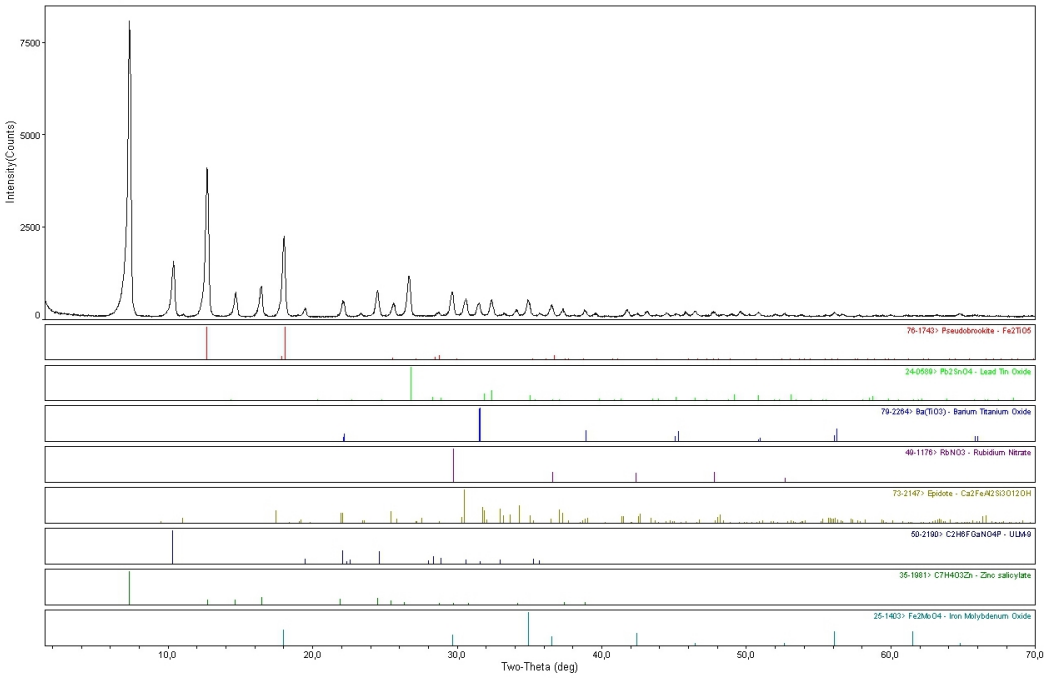

Figure 4.14. Qualitative XRD Results for ZIF-8 without Treatment.

Park *et al.* have reported [51]. The most important deduction however, is for deionized water. As mentioned, ZIF-8 has been proven to have a hydrophobic nature towards gaseous water. This is also the case in liquid water, as it has proved impossible to wet the surface of ZIF-8 using deionized water. It has been concluded that ZIF-8 cannot be impregnated using water in incipient-to-wetness impregnation method.

After these tests, it has been concluded that the only suitable solvent for MIL-53(Al) is deionized water. ZIF-8 has proven itself to be stable under IPA, acetone and hexane but deionized water cannot infiltrate the pores due to hydrophobic nature of the material. Tetraamineplatinum(II)nitrate has been found to be insoluble in IPA, acetone and hexane, therefore the idea of using ZIF-8 as a catalyst support has been scrapped. The project has moved forward with MIL-53(Al) as the only MOF material used in catalyst testing.

4.2. WGS over Pt Impregnated MIL-53(Al)

This section involves the parametric study of WGS over Pt/MIL-53(Al) catalysts with Pt loadings of 0.5wt.%, 1.0wt.% and 1.5wt.%. The experiments were performed in a 1/4 inch tubular quartz reactor, loaded with 100 mg catalyst. The reactions were conducted at 250 and 300 °C to compare temperature effect and S/C molar ratios of 1.67, 2.33 and 3 to investigate the steam effect on WGS. Total flow rate and N_2 flow rates were kept constant at 70 and 30 ml/min, respectively, as CO and H_2O were arranged to adjust to the desired S/C ratio given in Table 3.7. Figures 4.15, 4.16 and 4.17 give the results for 1.5%, 1.0% and 0.5% Pt loadings on MIL-53(Al), respectively for interpretation of temperature and S/C ratio effects. Figures 4.18 and 4.19 show the results for 300 and 250 °C to compare the Pt loading effect.

Observing Figure 4.15, it is obvious that at the highest S/C ratio, apparent CO conversion value has reached much higher values than the other ratios at both temperatures. At 250 °C the S/C ratios of 2.33 and 1.67 have very close conversion levels with the higher steam containing one having a small advantage, whereas at

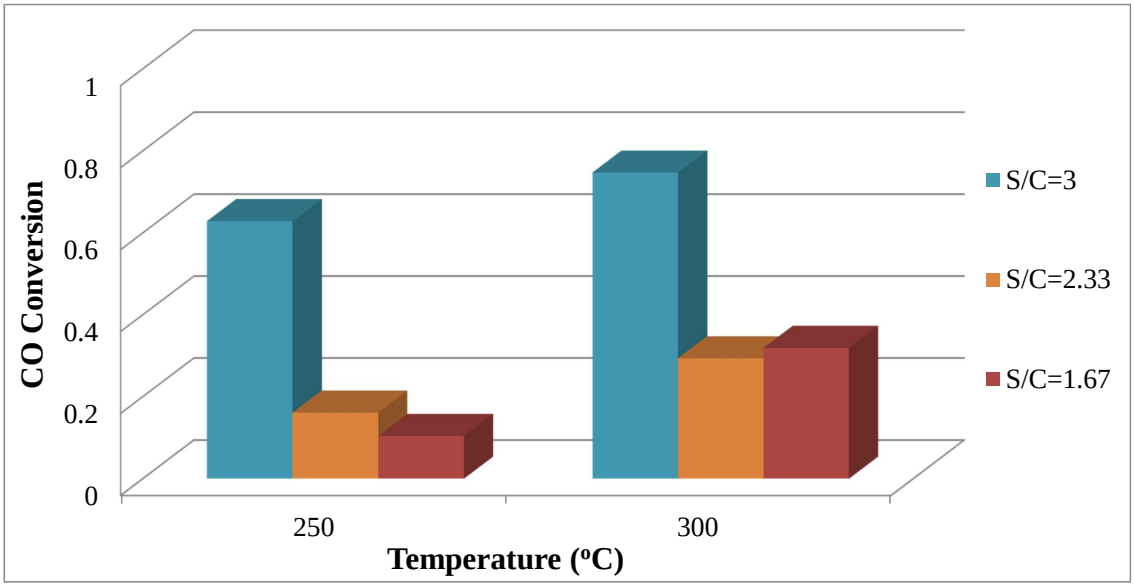

Figure 4.15. CO Conversion Values for 1.5wt.%Pt/MIL-53(Al).

300 °C the roles are reversed with S/C=1.67 having a marginal extra conversion. When comparing temperature effect on the outcome, all experiments have shown an increase in conversion value with increased temperature as expected due to increased WGS activity as a result of positive effect of temperature on reaction kinetics.

In Figure 4.16, experimental results of 1.0%Pt/MIL-53(Al) are given. The S/C ratio of 3 gives the highest amount of conversion for the catalyst at both temperatures. For the other S/C ratios, the conversion values are much lower, but in contrast to the results for 1.5% Pt/MIL-53(Al), at 250 °C the S/C ratio of 1.67 shows more activity then S/C=2.33. When the temperature is increased to 300 °C, S/C=2.33 case makes a jump in activity and almost doubles the conversion value of S/C=1.67. With the increase of temperature, CO conversions measured at S/C ratios of 3 and 2.33 show immense increase, whereas conversions observed at S/C=1.67 increases very slightly.

Figure 4.17 shows the results for the lowest Pt loading, 0.5%Pt/MIL-53(Al). The results show that again S/C ratio of 3 gives the highest conversion levels. In this case however, independent of temperature, CO conversion consistently decreases as the S/C ratio decreases, which is different than the cases of 1.5% and 1.0% Pt loading.

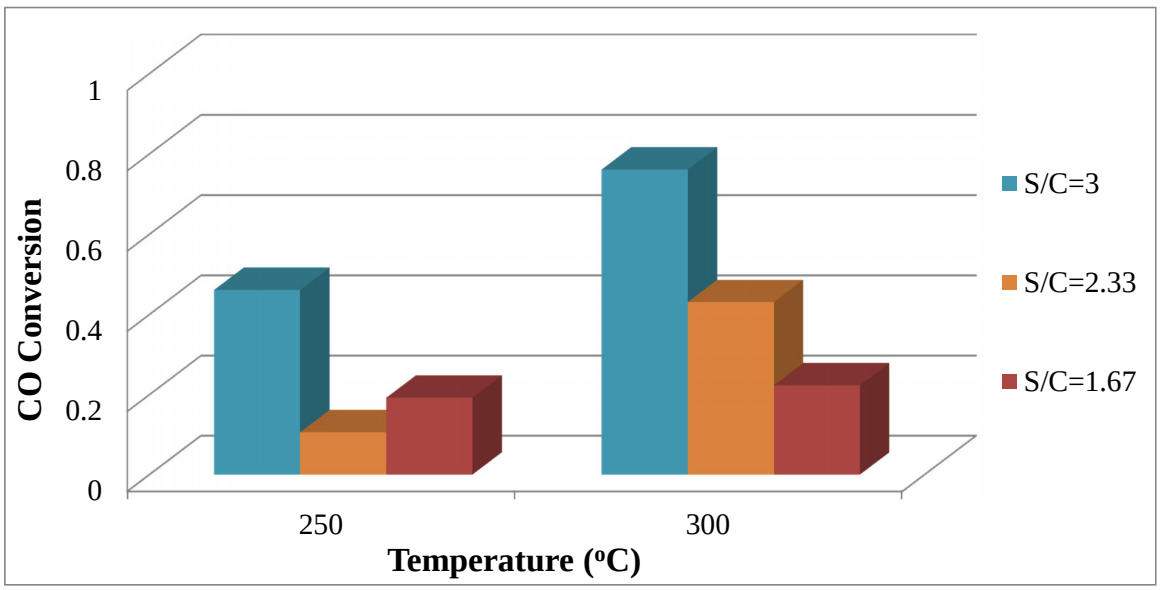

Figure 4.16. CO Conversion Values for 1.0wt.%Pt/MIL-53(Al).

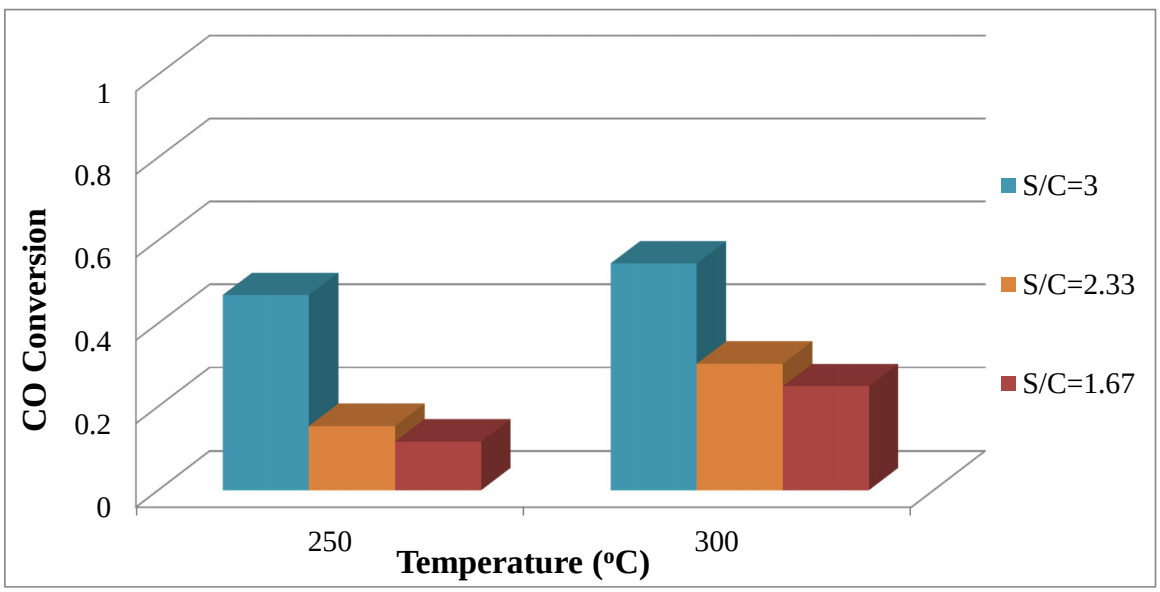

Figure 4.17. CO Conversion Values for 0.5wt.%Pt/MIL-53(Al).

Temperature effect stays the same, as the temperature is increased, the conversion values increased unanimously.

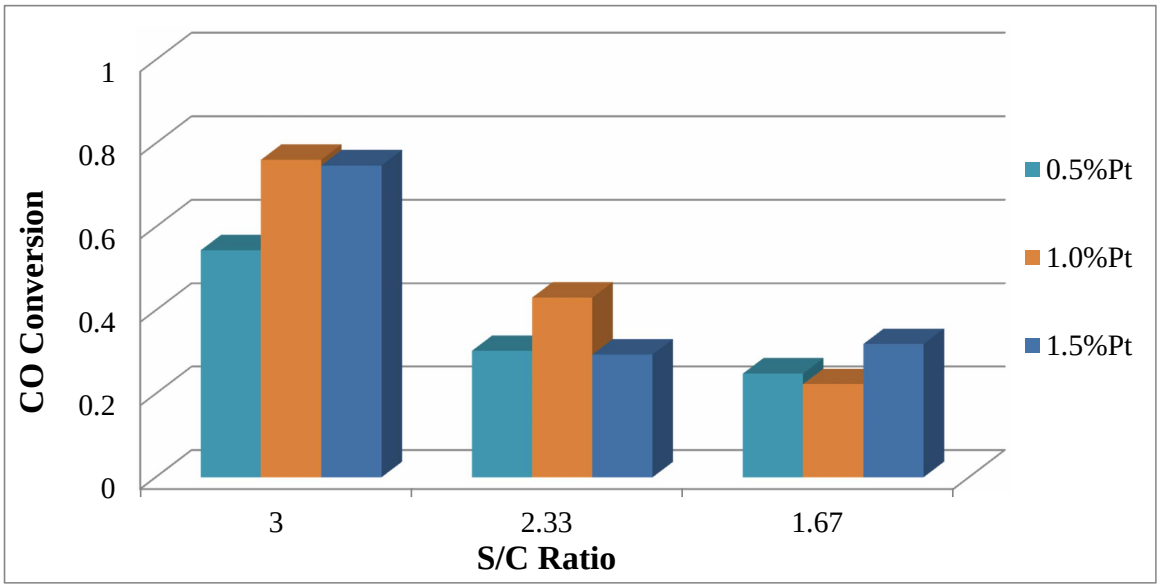

Figure 4.18. CO Conversion Values of Pt Supported MIL-53(Al) at 300°C.

Figures 4.18 and 4.19 are prepared to understand the of Pt loading effect on CO conversion at 300 and 250 °C. It can be observed that except for the S/C=3 case, the conversion results are within close proximity of each other. For S/C=3, it is logical to use 1.5wt.% metal loading at 250 °C but there is no added value in using 1.5wt.% Pt at 300 °C, therefore 1% will be sufficient at 300 °C. It can be seen through H_2 levels in Table 4.1 that the WGS reaction does not occur enough to justify the change in CO conversion levels. This is to say that WGS occurs at very low activity values on the MIL-53(Al) supported Pt catalyst and another mechanism is resulting in the decrease in CO output. The temperature increase magnifies the H_2 output in all cases, as the reaction proceeds faster at higher temperatures and Pt atoms become active above 250 °C. The increase in metal loading also affects the H_2 production in a positive manner.

Maximum conversion is achieved using 1.0wt.%Pt/MIL-53(Al) catalyst at 300 °C and S/C=3; with 1.5wt.%Pt/MIL-53(Al) at the same conditions closely following. The minimum CO conversions of 9% are obtained at 250 °C for S/C ratios of 2.33

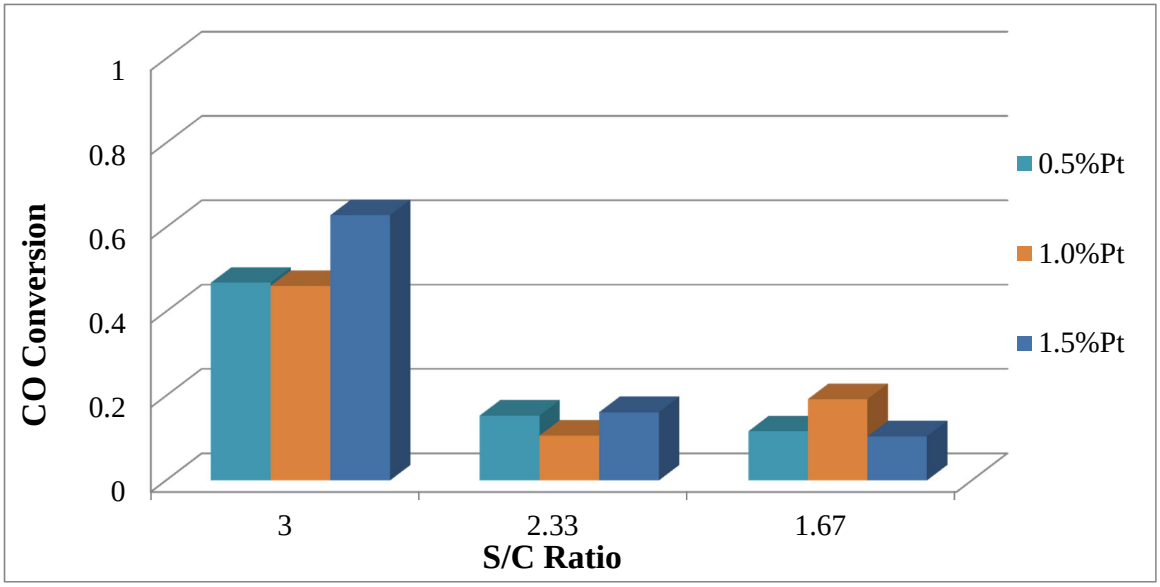

Figure 4.19. CO Conversion Values of Pt Supported MIL-53(Al) at 250°C.

and 1.67 S/C, respectively. For H_2 production, the highest values are obtained over 1.5wt.%Pt/MIL-53(Al) at 300 °C and at S/C=2.33, with S/C=3 as the runner up with a small margin. The lowest catalytic activity is observed over the 0.5wt.%Pt/MIL-53(Al) catalyst at 250 °C and 2.33 S/C ratio. The other S/C ratios are very close to this value, indicating that the dominant factors in play are temperature and metal loadings.

Examining Table 4.1, it is clear that the carbon balance is not uphold. CO_2 values in the product stream are not readable in the Carboxen 1000 column due to the very low concentrations. The reasons behind this behaviour is not apparent, and various estimates are made. The first logical explanation is that Boudouard reaction occurred on the catalyst surface. This is quickly dismissed as there is no sizeable CO_2 present in the product streams, which is a product of Boudouard reaction. The second explanation that comes to mind is the methanation reaction. This is also dismissed as there is no methane readings on the Porapak-Q column. Another explanation that is considered is the adsorption of CO on the support surface. The plausibility and discussion of this idea is given in Section 4.3.

Table 4.1. Experimental results of Pt impregnated MIL-53(Al).

Metal Loading (wt.%)	T (°C)	S/C Ratio	CO Feed vol.%	Product comp.(μmol/ml)	
				CO	H_2
1.5%	250	1.67	33.1	1210	2.05
		2.33	28.2	961	2.38
		3	24.8	380	3.704
	300	1.67	33.0	919	14.5
		2.33	28.0	809	18.4
		3	25.0	258	16.8
1.0%	250	1.67	33.0	1090	2.63
		2.33	28.2	1024	0.70
		3	24.8	551	3.18
	300	1.67	32.6	1036	5.84
		2.33	28.0	652	8.9
		3	25.0	244	7.78
0.5%	250	1.67	33.0	1193	1.09
		2.33	29.0	1005	0.69
		3	24.8	536	1.84
	300	1.67	32.6	1015	7.03
		2.33	29.2	833	6.06
		3	25.0	462	4.62

4.3. WGS over Alumina Supported Pt and MIL-53(Al) Combinations

In light of the low WGS activities obtained for MIL-53(Al) supported MOF's, the activity is sought to increase using 1.5wt.%Pt/CeO_x/Al_2O_3, a well established catalyst, physically together with MIL-53(Al) to better understand the mechanics in play when the MOF is present in the reactor. Three different configurations are experimented upon to find the effect of MIL-53(Al) on CO disappearance. First, 1.5wt.%Pt/CeO_x/Al_2O_3 is tested to find a basis to the catalytic activity of WGS for the parametric study. Second, MIL-53(Al) and 1.5wt.%Pt/CeO_x/Al_2O_3 are placed on top of each other in the reactor bed to observe the effect of MIL-53(Al) addition. Lastly, only MIL-53(Al) is inserted inside the reactor and tested at reaction conditions to find out about the effects of untreated, fresh MIL-53(Al) on CO.

Figure 4.20 shows the different catalyst configurations tested at 300 °C at various

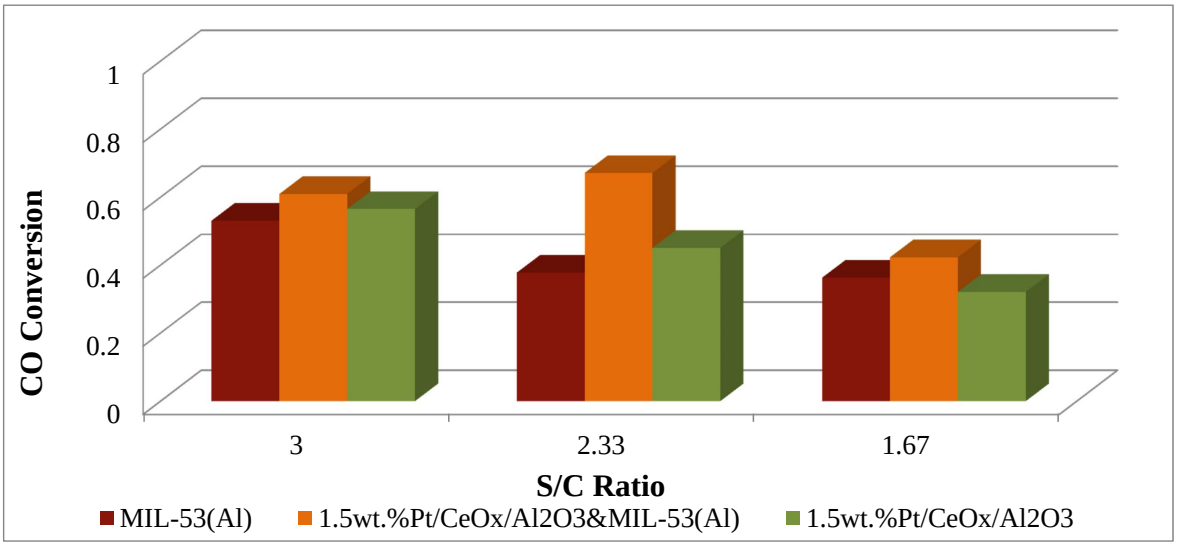

Figure 4.20. CO Conversion Values for Different Catalyst Configurations at 300°C.

S/C ratios. MIL-53(Al) results show the same trend as the Pt impregnated counterparts in Section 4.2. This means that the catalyst preparation method did not radically change the crystal structure of MIL-53(Al), which is in accordance with the XRD results. In Table 4.2, it can be seen that there is no WGS activity taking part in MIL-53(Al) experiments, as there is absolutely no H_2 in the product stream. Taking a look at 1.5wt.%Pt/CeO_x/Al_2O_3 results, one can easily see that an increase in S/C ratio increases the WGS activity. It is important to note that the carbon balance for 1.5wt.%Pt/CeO_x/Al_2O_3 catalyst holds at every experiment, meaning that the conversion values stem from WGS activity directly. The combined reactions hold interest due to the effect of fresh MIL-53(Al) added over a working WGS catalyst. It is observed that the addition of MIL-53(Al) increases the apparent conversion value for all runs. Table 4.2 clearly shows that there are no significant differences in H_2 production between 1.5wt.%Pt/CeO_x/Al_2O_3 + MIL-53(Al) and 1.5wt.%Pt/CeO_x/Al_2O_3 runs. The combined effect of MIL-53(Al) and 1.5wt.%Pt/CeO_x/Al_2O_3 increases the apparent conversion, but it is evident that this does not occur in an additive fashion, meaning that the individual CO conversion values do not add up to the combined CO value. It is interesting to note that while MIL-53(Al) and 1.5wt.%Pt/CeO_x/Al_2O_3 both have their highest conversion values at S/C=3, the highest conversion obtained for the combined

case is at S/C=2.33.

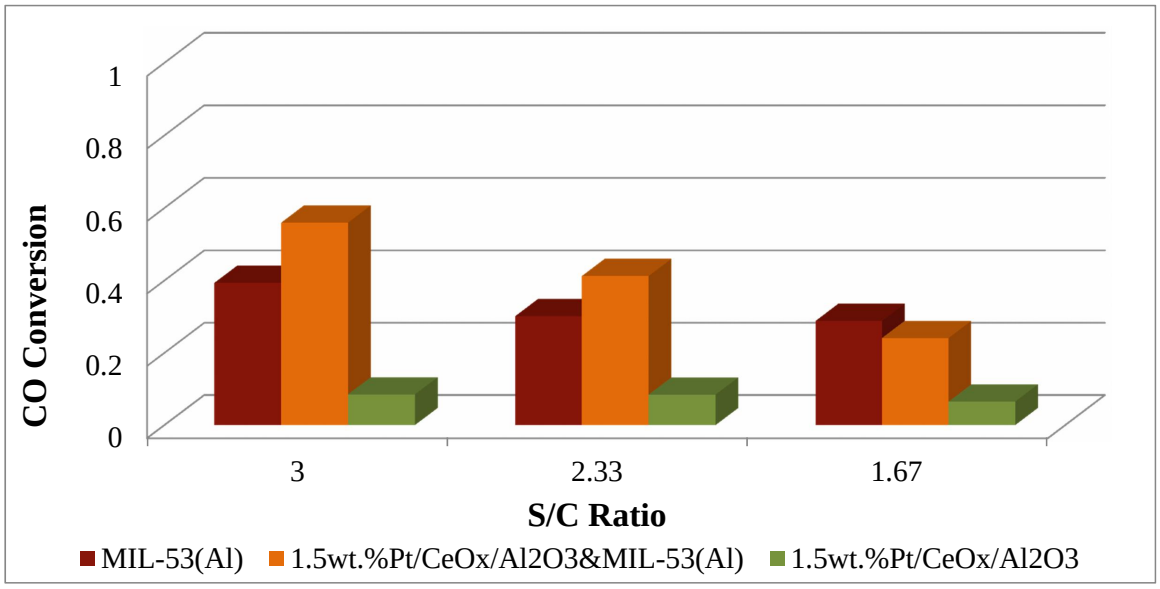

Figure 4.21. CO Conversion Values for Different Catalyst Configurations at 250°C.

Figure 4.21 shows the results for 250 °C. It can be seen that 1.5wt.%Pt/CeO_x/Al_2O_3 catalyst has very low conversion values. This is due to Pt atoms being inactive at low temperatures, as explained in the literature. MIL-53(Al) conversion values create the major CO conversion values in this experiment set. The values are again in accordance with the results from Section 4.2, with S/C=3 ratio showing the highest conversion. It is important to note that the combined case for S/C=1.67 gives a lower activity value than its MIL-53(Al) counterpart. This trend change is attributed to the combination of CO uptake, low temperature and low steam ratio effects, which leaves the catalyst with low CO and H_2O in the stream. This could, due to thermodynamic limitations, increase the rate of reverse WGS reaction, decreasing the CO conversion level.

Table 4.2 gives an overview the experimental results of the catalyst configurations studied in this section. 1.5wt.%Pt/CeO_x/Al_2O_3 catalyst performance shows that the reaction justifies carbon balance, and increasing the temperature from 250 to 300 °C radically increases the WGS activity of the catalyst. This is reported numerous times in literature. Another point to make is the inactivity of MIL-53(Al) in WGS reaction when no Pt is deposited on it. This inert position, however, does not explain why there

are large chunks of carbon materials missing when the reaction is conducted. Also, SEM and EDX characterizations are conducted to further understand the surface of MIL-53(Al) and possibly interpret the results. Several extra tests are also carried out to find out more about the possible root causes of the results, and are explained in Section 4.5.

Table 4.2. Experimental results of various catalyst configurations.

Catalyst	T (°C)	S/C Ratio	CO Feed vol.%	Product comp. (μmol/ml)	
				CO	H_2
MIL-53(Al)	250	1.67	32.8	961	0
		2.33	28.2	798	0
		3	25.2	618	0
	300	1.67	33.0	860	0
		2.33	28.2	713	0
		3	25.0	479	0
MIL-53(Al) + 1.5wt.%Pt/CeO_x/Al_2O_3	250	1.67	33.3	1024	99.2
		2.33	28.0	673	95.5
		3	25.1	450	90.6
	300	1.67	32.6	779	461
		2.33	28.0	372	464
		3	25.0	400	526
1.5wt.%Pt/CeO_x/Al_2O_3	250	1.67	33.4	1262	69.2
		2.33	28.6	1048	101.
		3	25.0	936	82.9
	300	1.67	32.3	917	443
		2.33	28.2	629	492
		3	25.1	674	516

The highest CO conversion is 67% observed in the experiments is obtained in combined testing of the materials, at 300 °C and S/C=2.33. The lowest conversion of CO conversion of 8% is obtained for the standalone 1.5wt.%Pt/CeO_x/Al_2O_3 catalyst at 250 °C throughout all S/C ratios, due to the inactivity of Pt atoms at low temperatures. Increasing S/C resulted in more CO being converted in the experiments without fail. 1.5wt.%Pt/CeO_x/Al_2O_3 also showed higher WGS activity under steam-rich conditions. This is mainly due to the kinetics of WGS over 1.5wt.%Pt/CeO_x catalysts, as literature shows that kinetics with respect to CO is zero order, whereas H_2O is first order, leading to increased WGS activity at higher steam concentrations.

4.4. Catalyst Characterization

Scanning Electron Microscopy (SEM) and Energy Dispersive X-Ray Spectroscopy (EDX) surface characterization techniques are conducted over various stock, fresh, and spent MIL-53(Al) catalysts to find out more about the disappearance of CO in the experiments reported in Sections 4.2 and 4.3. A fresh MIL-53(Al) is imaged for comparison purposes in Figure 4.22.

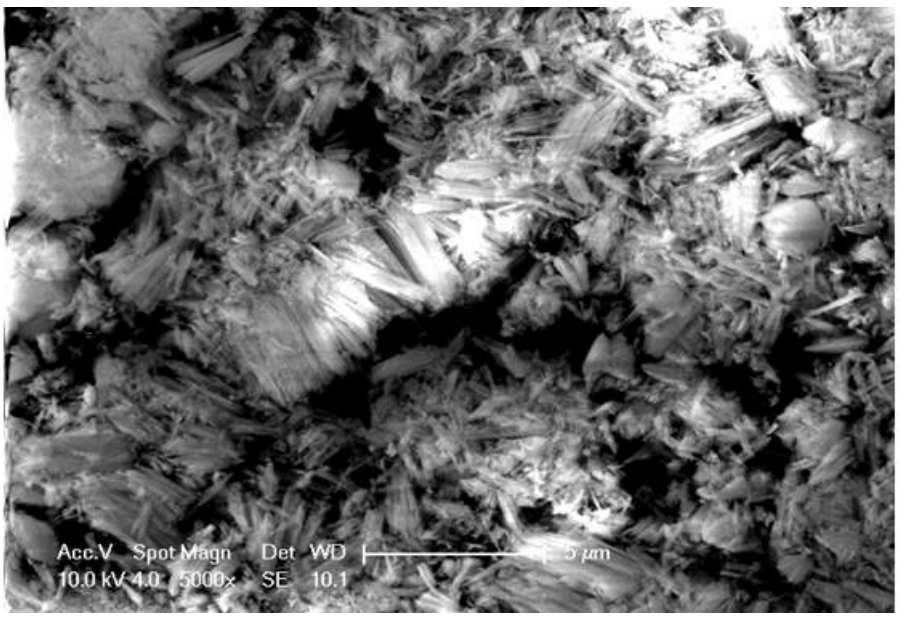

a MIL-53(Al) Magnified 5000x

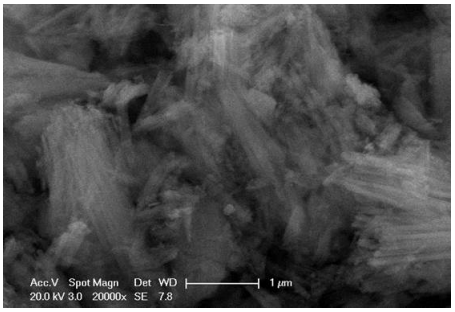

b MIL-53(Al) Magnified 20000x

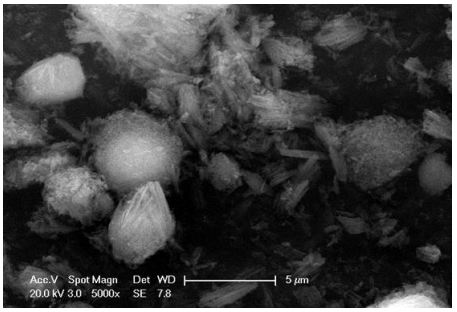

c MIL-53(Al) Magnified 5000x

Figure 4.22. SEM Results of MIL-53(Al).

It is seen that the surface of MIL-53(Al) is composed of long and thin, sharp pointy structures. This is consistent with the thought of a framework structure. The material does not conduct electricity well, hence the voltage is increased to get clearer images. Since there are no special atoms that are being tested for here, this serves to

demonstrate the intact structure of MIL-53(Al). The EDX analysis of these particles revealed that apart from Al, C, O and H atoms that are naturally found in MIL-53(Al), trace amounts of sulfur is present.

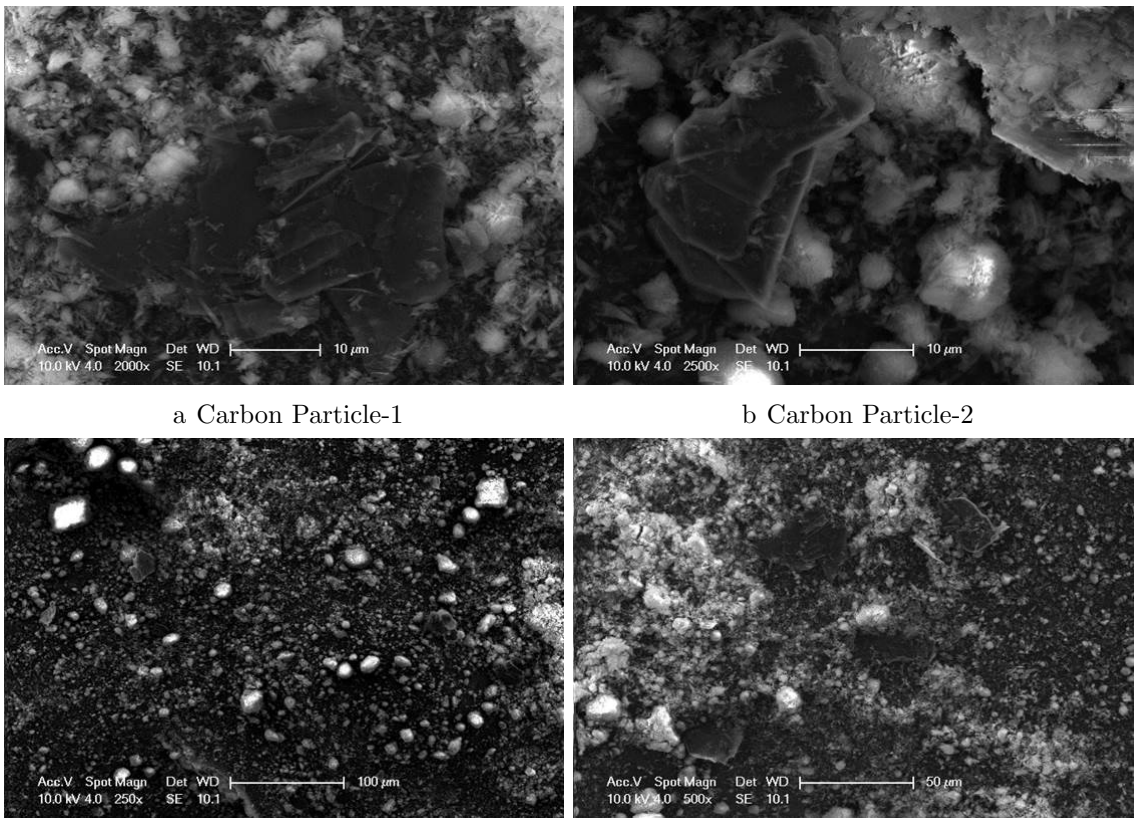

a Carbon Particle-1 b Carbon Particle-2

c Carbon Species inside MIL-53(Al)-1 d Carbon Species inside MIL-53(Al)-2

Figure 4.23. Carbon species in MIL-53(Al).

SEM imaging revealed that on fresh MIL-53(Al) particles, carbon species in many different sizes and shapes are present. As seen in Figure 4.23, the species are dark and can conduct electricity. EDX analysis on these particles revealed that they completely consisted of carbon atoms. It is unknown whether these particles had any affect on the experiment results, they are obvious contaminations to the testing system. In Figure 4.23d, carbons as large as MIL-53(Al) particles, can be observed. It is unknown whether this is the result of a side-reaction occurring in the preparation of MIL-53(Al).

The SEM imaging of fresh (i.e. reduced under H_2 flow) 1.0%Pt/MIL-53(Al) in Figure 4.24 clearly shows the Pt clusters impregnated over MIL-53(Al). The cluster sizes are found to be between 7.5 and 13 nm, with some agglomeration few and far

between, such as the right hand corner of Figure 4.24d. It should be noted that even with this high dispersion, the catalytic activity of Pt/MIL-53(Al) catalysts are found to be very poor in WGS. This means that another promoter, such as ceria, might be needed to increase the catalytic activity of Pt atoms on the surface through redox mechanism.

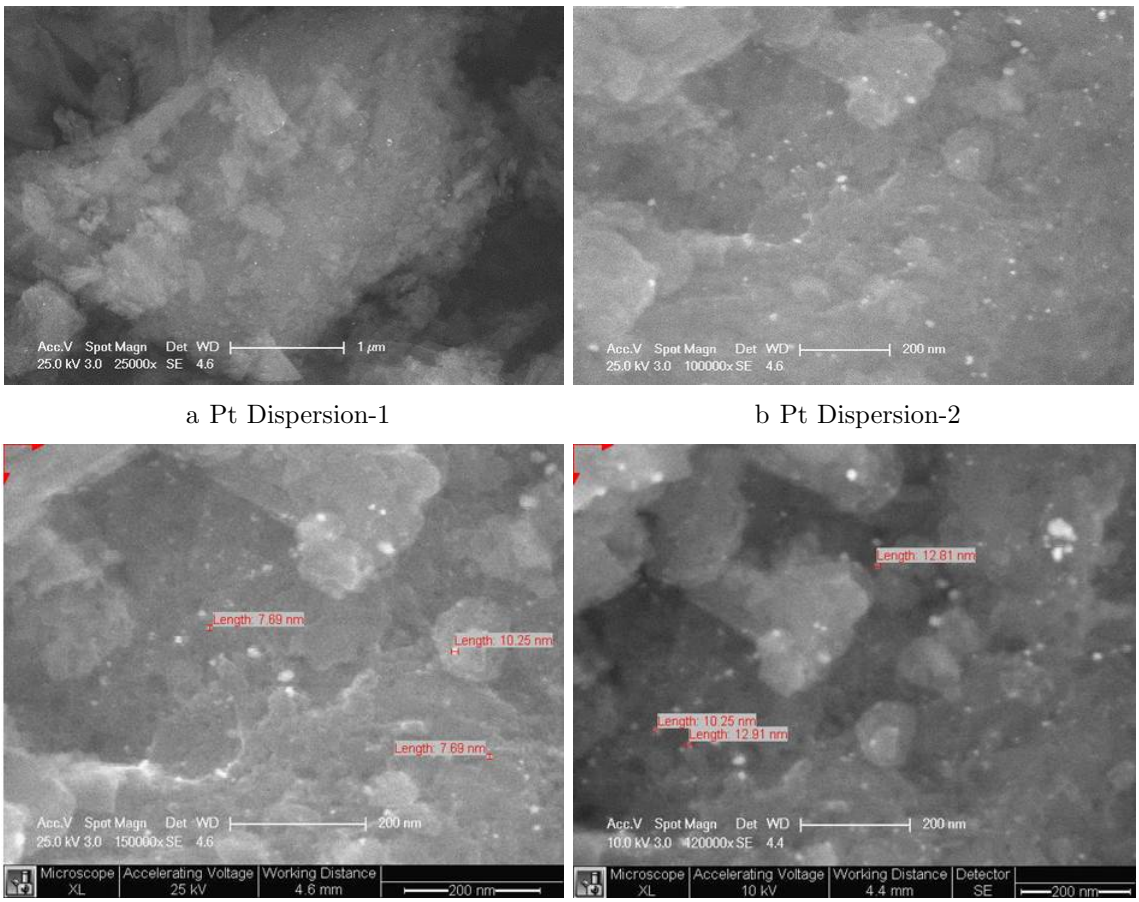

a Pt Dispersion-1 b Pt Dispersion-2

c Pt Cluster Sizes-1 d Pt Cluster Sizes-2

Figure 4.24. SEM Imaging of 1.0%Pt/MIL-53(Al) Before Reaction.

Figure 4.25 shows 1.0%Pt/MIL-53(Al) after reaction. The clusters of Pt are found to be bigger than the ones observed over the fresh catalyst, with sizes ranging from 15 to 25 nm perhaps due to sintering during the reaction. Figure 4.25c shows MIL-53(Al) surface after reaction, and no severe change in the shapes of particles can be observed other than the fact that particles seem to be more round shaped this time, likely due to the impregnation process. Figure 4.25d shows the carbon species already found on fresh MIL-53(Al). It is noted that this is the largest found on the SEM images, but this does not necessarily mean that the particle got larger during the reaction, and

may be just a coincidence.

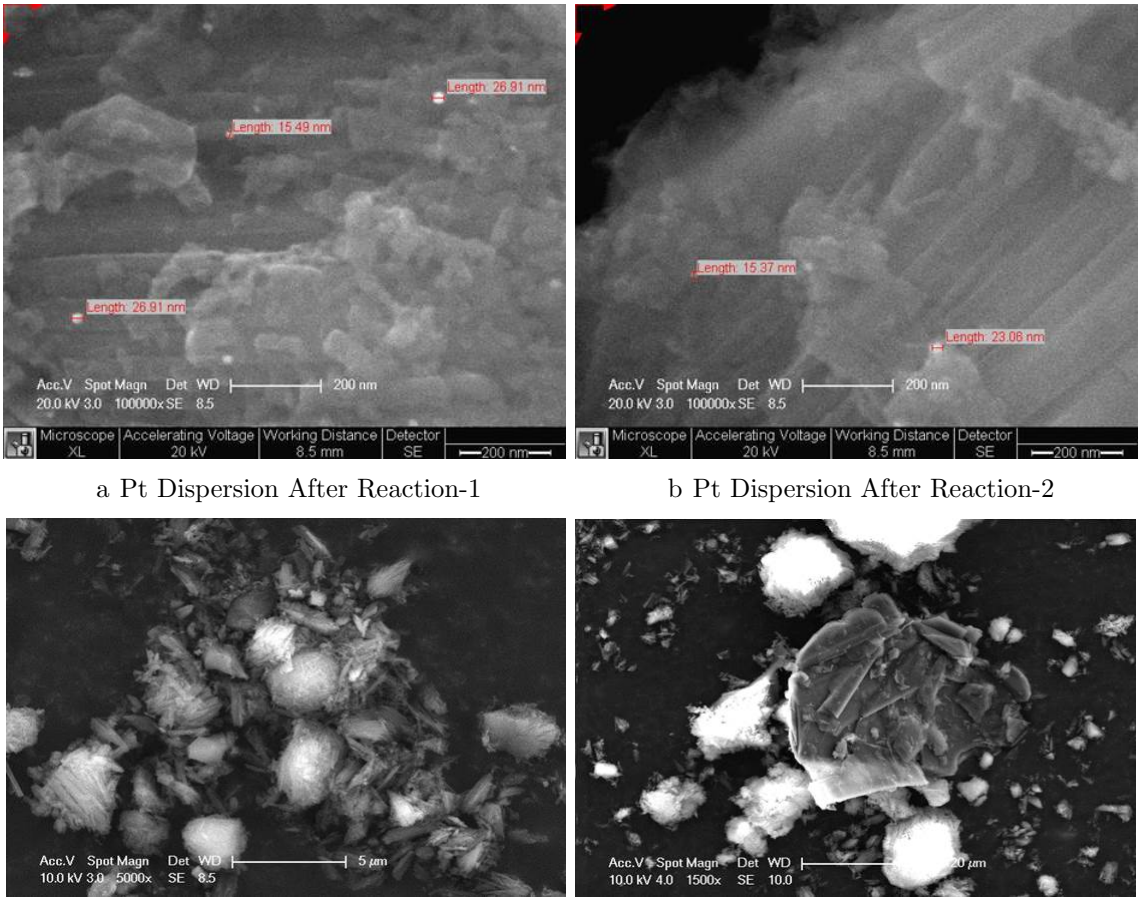

a Pt Dispersion After Reaction-1

b Pt Dispersion After Reaction-2

c Surface of MIL-53(Al) after Reaction

d Carbon Species in spent MIL-53(Al)

Figure 4.25. SEM Imaging of 1.0%Pt/MIL-53(Al) After Reaction.

The SEM imaging shows that there are contaminants mixed with MIL-53(Al) produced commercially. It is imperative to understand if these carbon species caused the erratic behaviour observed in CO decrease. Strong adsorption of CO on the surfaces of MIL-53(Al) or these carbons may occur, but there should be limit to how much these materials can adsorb until they reach saturation. A 24 hour time-on-stream test is conducted to test this hypothesis and its results are given in Section 4.5. Also, the sulfur found on the surface of MIL-53(Al) is alarming. This is another type of contaminant that should not be present as there are no sulfur species used in the synthesis of MIL-53(Al). It is impossible to know whether the sulfur on the surface of MIL-53(Al) has played any role in the inactivity of Pt atoms in WGS reaction, or the possible CO bonding or adsorption.

4.5. Miscellaneous Testing

This section contains the outcomes of various experiments conducted to provide further insight into the interaction between MIL-53(Al) and CO.

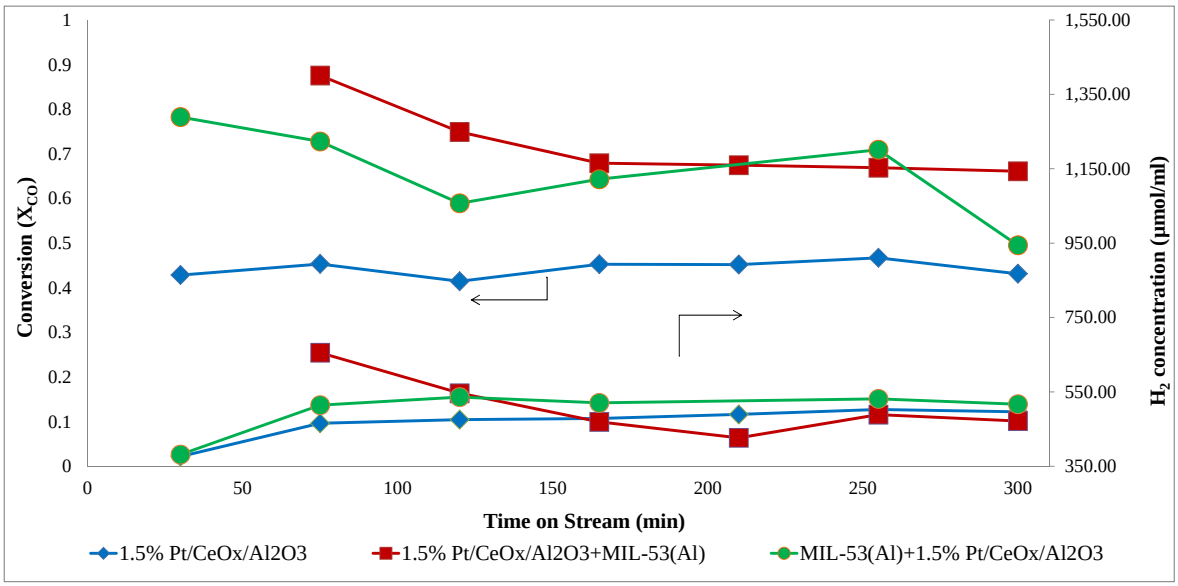

Figure 4.26. CO Concentration Values at Various Catalyst Configurations.

The first experiment is conducted to understand whether the physical locations of MIL-35(Al) and 1.5wt.%$Pt/CeO_x/Al_2O_3$ in the tubular reactor affected the outcome in any way under identical testing conditions. Outcomes of these experiments are given in Figure 4.26. It is found that it did not matter if MIL-53(Al) is positioned on top of or under the 1.5wt.%$Pt/CeO_x/Al_2O_3$ catalyst layer. The H_2 concentrations in both cases, and over the standalone 1.5wt.%$Pt/CeO_x/Al_2O_3$ catalysts are found to be nearly the same. The conversion values are approximately equal to each other in the case of coupled experiments, but is significantly lower when standalone 1.5wt.%$Pt/CeO_x/Al_2O_3$ is used. This behaviour is also identified and expanded upon in Section 4.3.

The second test is done to understand under what conditions CO is held. Figure 4.27 shows the change in CO concentration at various start-up points when in contact with 1.0% MIL-53(Al). The test, involving a feed with 30% CO and 70% N_2 by volume, is conducted in a single run, over the same catalyst. The second batch of

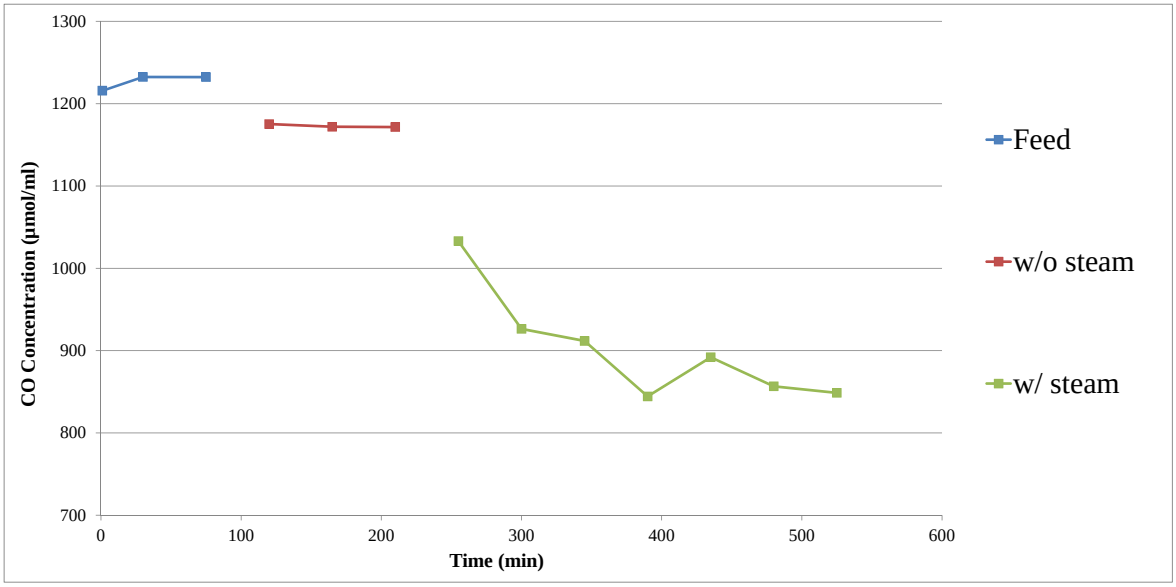

Figure 4.27. CO Concentration Values Under 300 °C and S/C=2.33.

data points show the progression when CO/N_2 mixture is sent over the catalyst. There is some decrease in CO concentration, but is limited to ca. 1%. The largest set of data is for when the steam is sent together with CO and N_2, starting at 255 minutes. A sharp decline in CO concentration on the product stream is observed, with almost no H_2 appearing. This test shows that the decrease in CO is somewhat related to the steam in the stream. This makes sense with the data obtained for MIL-53(Al) in the parametric studies, where the highest conversion values were obtained at the highest S/C ratio of 3.

The third test is done to understand if a similar effect of CO disappearance on MIL-53(Al) occurs for H_2. In Figure 4.28, it can be clearly seen that H_2 concentration does not decrease when it is sent together with N_2 and steam. This means there are no losses to the H_2 produced in the reactions when MIL-53(Al) is present.

The last test is conducted to find out about the stability of the catalyst, and the duration of the 'CO uptake' effect. The catalyst is subjected to a 24 hour test under S/C=3 and 300 °C. As illustrated in Figure 4.29, although there are some oscillations, the apparent conversion and H_2 concentration curves stay horizontal.

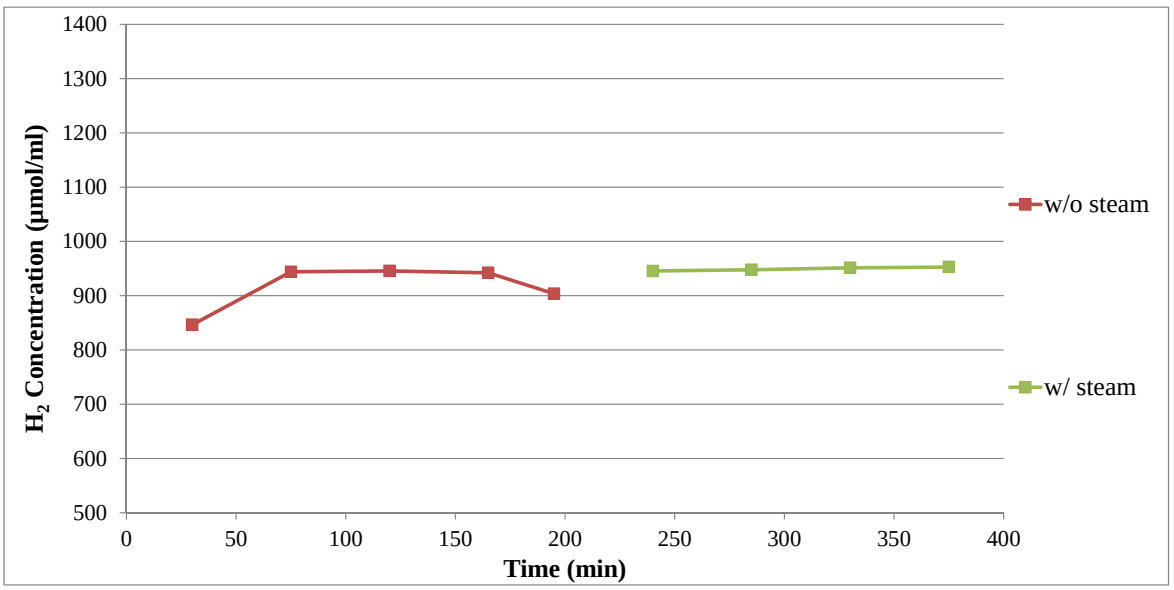

Figure 4.28. H_2 Concentration Values Without and With Steam on MIL-53(Al).

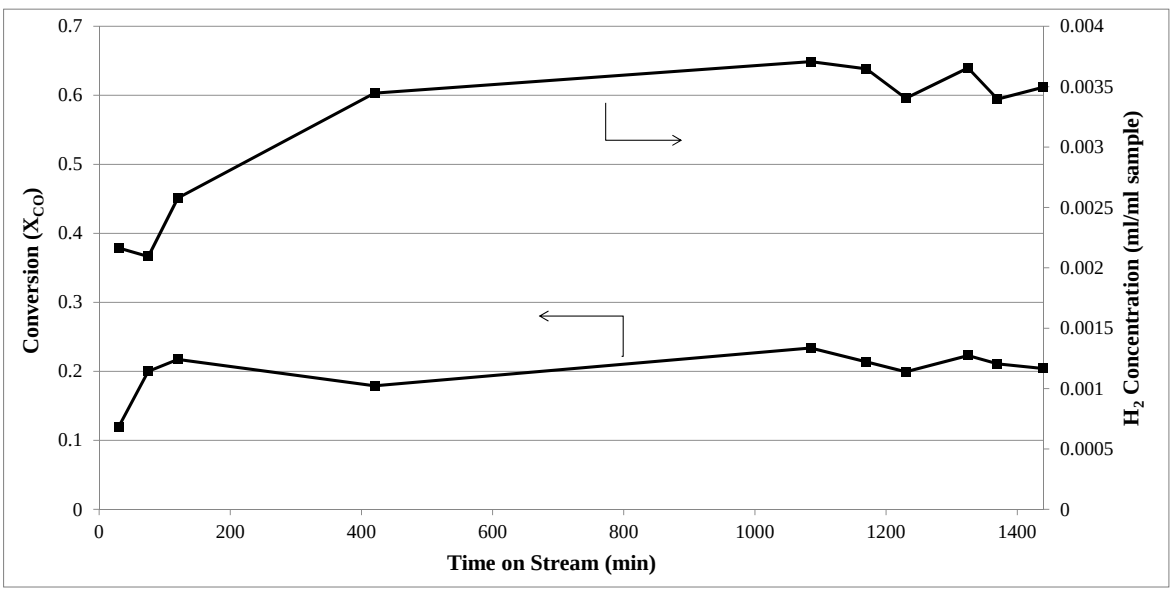

Figure 4.29. 24 Hour Test Run on 1.0%Pt/MIL-53(Al).

5. CONCLUSIONS AND RECOMMENDATIONS

5.1. Conclusions

The main aim of this study is to observe the effects of using a MOF material, MIL-53(Al) on CO conversion in WGS reaction at low temperatures and at various steam-to-carbon ratios. The testing is carried out with 0.5%Pt/MIL-53(Al), 1.0%Pt/MIL-53(Al) and 1.5%Pt/MIL-53(Al) catalysts. Apart from using it as a support, MIL-53(Al) is physically coupled to 1.5wt.%1.5%Pt/CeO_x/Al_2O_3, a well known WGS catalyst. In order to understand the effect of water, and the long term sustainability of the results, some specialized experiments are conducted. Catalyst surface characterization is done using SEM and EDX, while XRD is used to find out more on MIL-53(Al) and ZIF-8 stabilities in various solvents. Pt/MIL-53(Al) catalysts are prepared by incipient-to-wetness impregnation method, while 1.5wt.%Pt/CeO_x/Al_2O_3 catalyst is prepared through sequential impregnation. The conclusions of this study are summarized as follows:

- XRD results show that MIL-53(Al) is only stable under deionized water, and undergoes minimal structural changes when subjected to IPA. Acetone, hexane and methanol are found to be disruptive of MIL-53(Al)'s structural properties.
- ZIF-8 is found to be stable when contacted with IPA, acetone and hexane. Due to the hydrophobic nature of the material, deionized water cannot infiltrate the pores, making incipient-to-wetness impregnation impossible for ZIF-8 using deionized water.
- The highest conversion on MIL-53(Al) supported Pt catalysts is found to be 72% for 1.0wt.%Pt/MIL-53(Al), at 300 °C and S/C=3. Closely following is 1.0wt.%Pt/MIL-53(Al), with 70%. It is observed that S/C ratio and temperature dominated apparent conversion values, but Pt loading did not have a clear effect. H_2 production is found to be highest for 1.5wt.%Pt/MIL-53(Al) at 300 °C and S/C=2.33, with 18.4 μmol/ml. It is noted that this value is too low to justify

the high conversions observed. The data shows that Pt loading and temperature have a positive effect on H_2 production and generally higher S/C ratios lead to higher catalytic activities.

- Catalyst configuration testing is carried out to understand the effect of fresh MIL-53(Al) more clearly. Experiments show that MIL-53(Al) is completely inert in WGS reaction, as no H_2 is produced in solo testing. Even with the lack of WGS, product stream had less CO than the feed, meaning another mechanism is at work regarding the interaction of CO and MIL-53(Al). As expected, the highest WGS activity is found in the experiment involving 1.5wt.%$Pt/CeO_x/Al_2O_3$, whether coupled or not with MIL-53(Al), at 300 °C and S/C=3. WGS activity is enhanced by temperature increase, as Pt is inactive at low temperatures, and it is observed that higher steam amounts in the feed stream increases the activity, which is consistent with the literature. Higher metal loading also increases the WGS activity, though only for a marginal amount. The highest CO conversion of 67% is obtained in combined MIL-53(Al) and 1.5wt.%$Pt/CeO_x/Al_2O_3$ configuration, at 300 °C and S/C=2.33. It is observed that coupling the materials give higher conversion values than solo testing.
- SEM imaging on MIL-53(Al) show that there are carbon species mixed together with MIL-53(Al). Also, sulfur is detected on MIL-53(Al) surface. It is unknown whether these contaminants had an effect on the inactivity of Pt/MIL-53(Al) catalyst towards WGS, or the erratic behaviour of CO disappearance over MIL-53(Al). Fresh and spent catalyst imaging shows that Pt clusters sizes increase from 7.5-13 nm to 15-25 nm, indicating that sintering is in effect during the reaction.
- Miscellaneous tests are conducted to better understand the effect of MIL-53(Al) on CO uptake from the feed stream. The position of 1.5wt.%$Pt/CeO_x/Al_2O_3$ over or under MIL-53(Al) is found to not affect the outcome, either in H_2 production values or in CO conversion terms. It is observed that the addition of steam in the feed stream caused the decrease of CO in the feed stream. H_2 is not affected by the mechanism that effects CO over ML-53(Al). A 24 hour test showed that the effect of MIL-53(Al) is stable, with minor fluctuations.

5.2. Recommendations

According to the results of the present study, the following recommendations are believed to be beneficial for future improvements:

- WGS reaction should be studied under reformate conditions, as H_2 and CO_2 are both known to inhibit the reaction through surface adsorption and reverse reaction due to equilibrium.
- Catalyst preparation methods other than incipient-to-wetness impregnation, such as chemical vapour deposition and solid grinding, both of which provide improved metal dispersions, should be investigated. Use of these techniques will also allow the use of ZIF-8 as a potential support for the WGS reaction.
- As an active metal, Au should be researched in conjunction with MOF's. It is reported that very low cluster sizes can be achieved using Au/MIL-53(Al), which is a prerequisite when using Au for catalysis [50]. Also, the proven low activation energy of Au in WGS catalysis can lead to even lower reaction temperatures, resulting in a larger array of suitable MOF's.
- Impregnating ceria over MOF surface would act as a medium for the redox mechanism in WGS to proceed, potentially elevating the activity of the reaction.
- Instead of buying commercially produced MOF's, synthesizing them in the labs can open the road to engineering the materials to the needs of the reaction and is highly recommended.

APPENDIX A: CALIBRATION CURVES OF MFC's

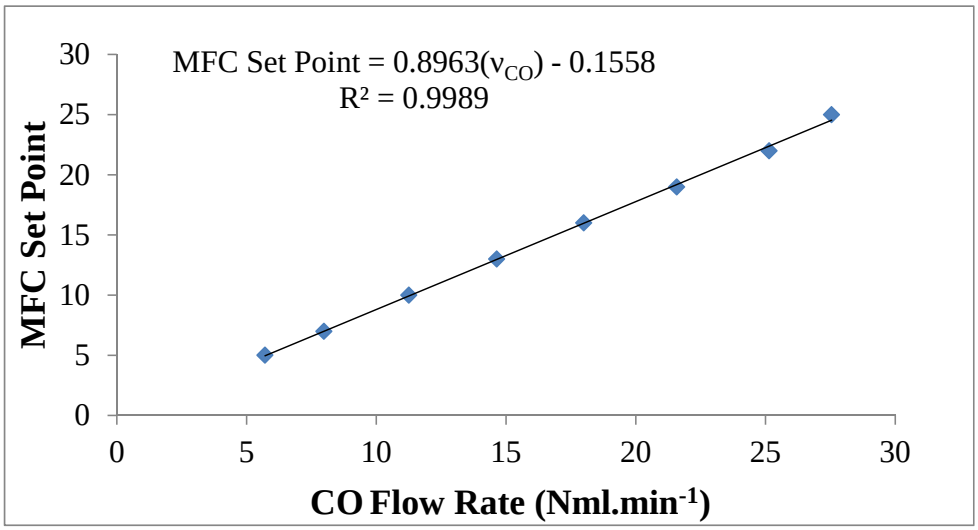

Figure A.1. MFC Calibration Curve for CO.

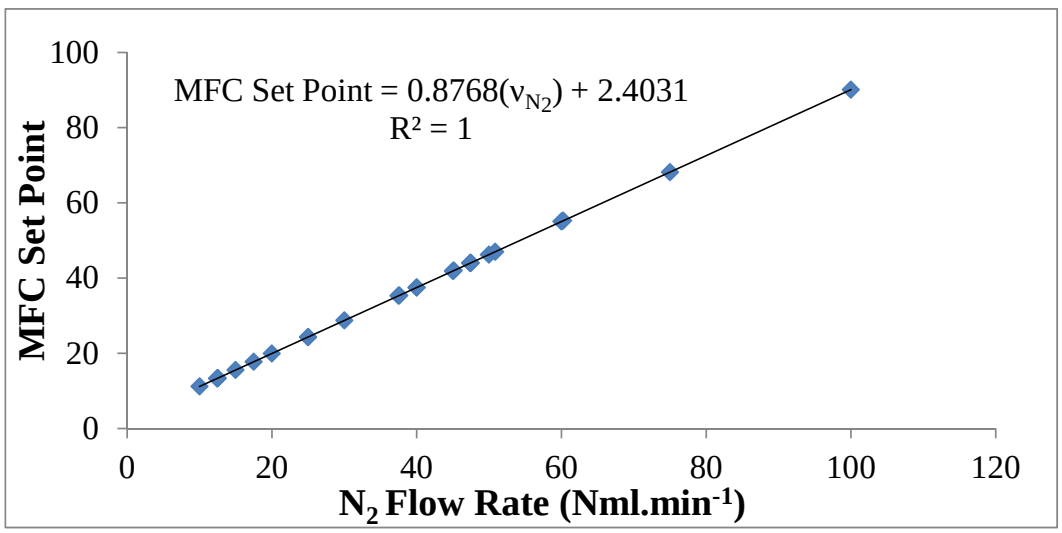

Figure A.2. MFC Calibration Curve for N_2.

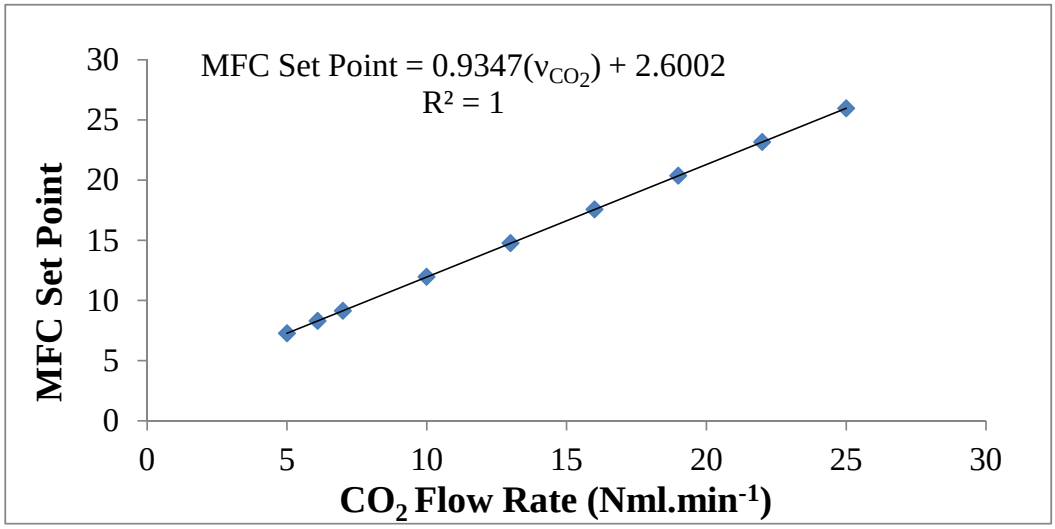

Figure A.3. MFC Calibration Curve for H_2.

APPENDIX B: CALIBRATION CURVES OF GC'S

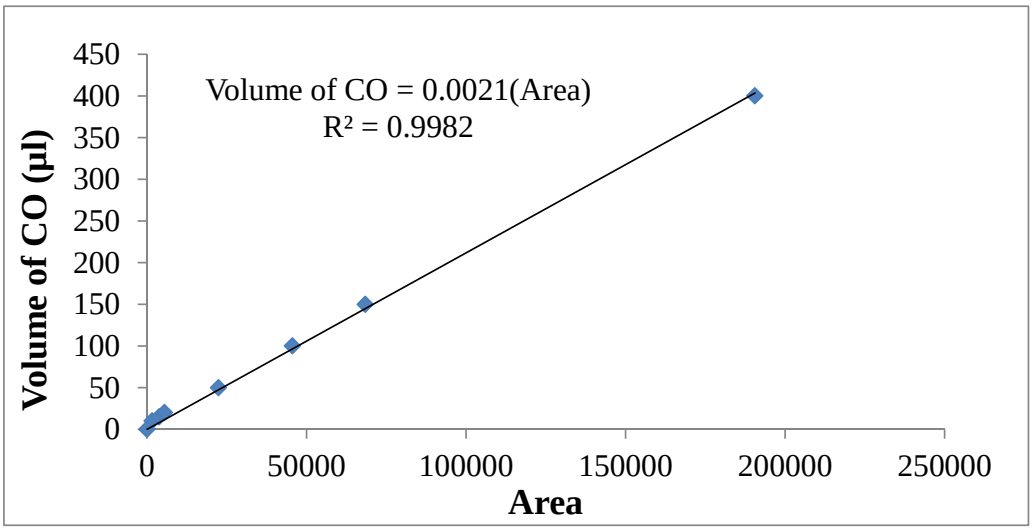

Figure B.1. GC Calibration Curve for CO.

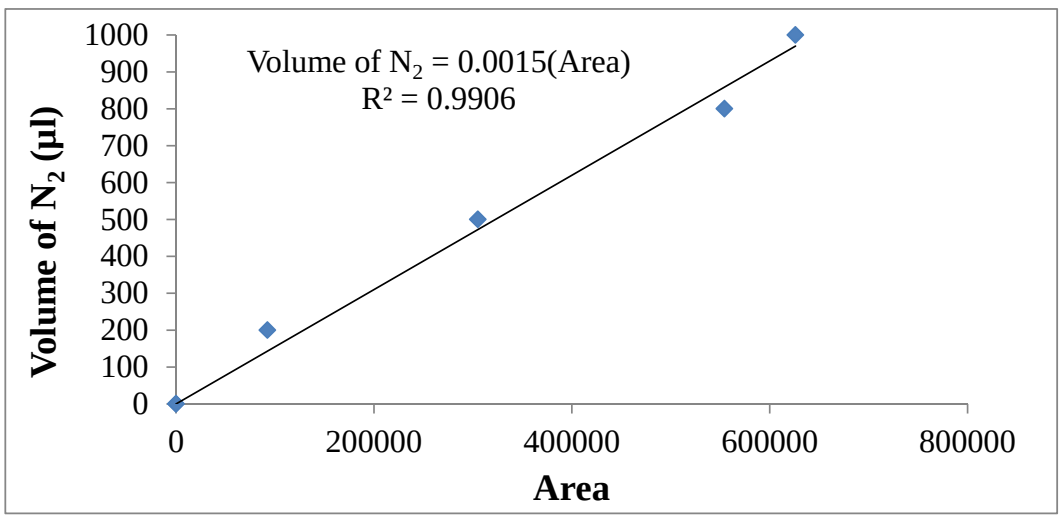

Figure B.2. GC Calibration Curve for N_2.

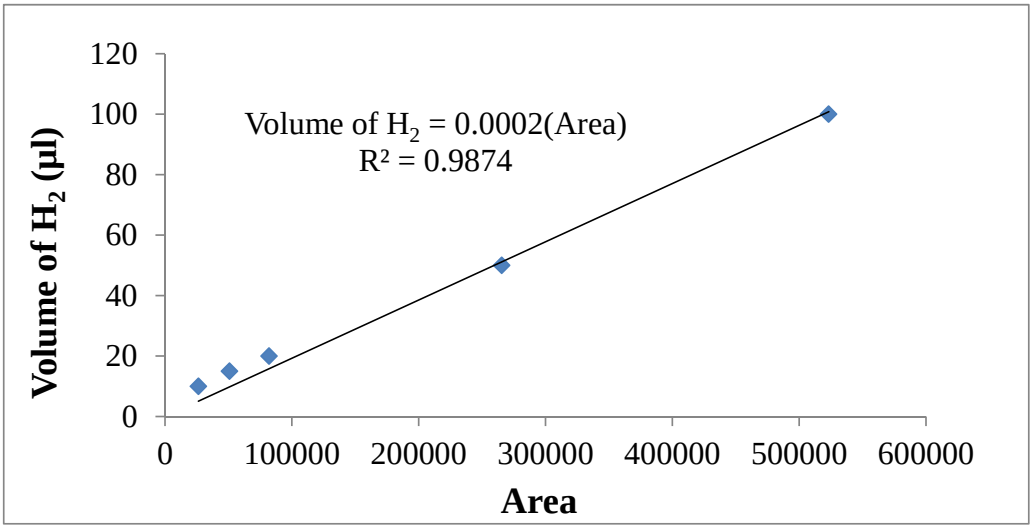

Figure B.3. GC Calibration Curve for H_2.

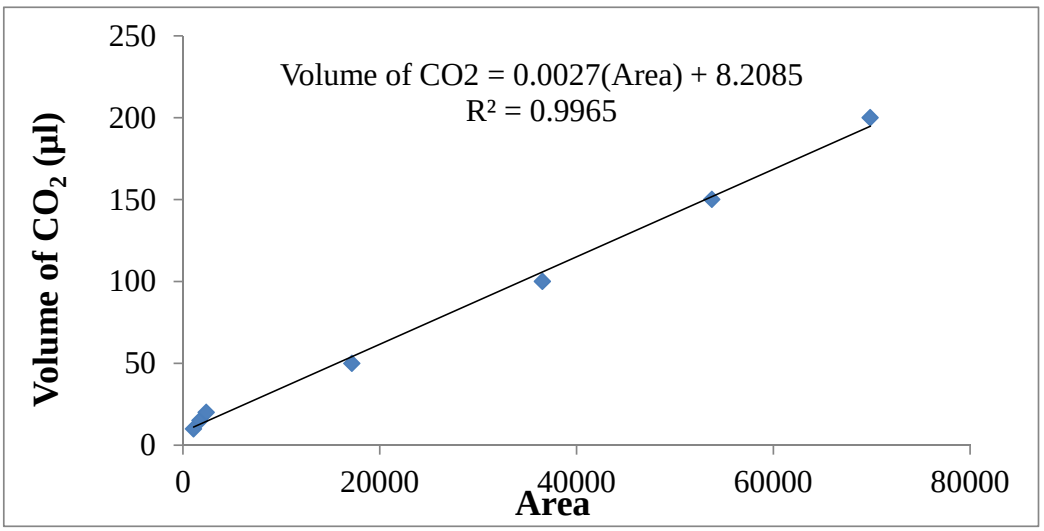

Figure B.4. GC Calibration Curve for CO_2.

REFERENCES

1. Chen, W.-H., T.-C. Hsieh, and T. L. Jiang, "An Experimental Study on Carbon Monoxide Conversion and Hydrogen Generation from Water Gas Shift Reaction", *Energy Conversion and Management*, Vol. 49, No. 10, pp. 2801 – 2808, 2008.

2. Zalc, J. and D. Loffler, "Fuel Processing for PEM Fuel Cells: Transport and Kinetic Issues of System Design", *Journal of Power Sources*, Vol. 111, No. 1, pp. 58 – 64, 2002.

3. Lenite, B. A., C. Galletti, and S. Specchia, "Studies on Au Catalysts for Water Gas Shift Reaction", *International Journal of Hydrogen Energy*, Vol. 36, No. 13, pp. 7750 – 7758, 2011.

4. Farrusseng, D., S. Aguado, and C. Pinel, "Metal-Organic Frameworks: Opportunities for Catalysis", *Angewandte Chemie International Edition*, Vol. 48, No. 41, pp. 7502–7513, 2009.

5. Lee, J., O. K. Farha, J. Roberts, K. A. Scheidt, S. T. Nguyen, and J. T. Hupp, "Metal-Organic Framework Materials as Catalysts", *Chemical Society Reviews*, Vol. 38, pp. 1450–1459, 2009.

6. Kirubakaran, A., S. Jain, and R. Nema, "A Review on Fuel Cell Technologies and Power Electronic Interface", *Renewable and Sustainable Energy Reviews*, Vol. 13, No. 9, pp. 2430 – 2440, 2009.

7. Turner, J. A., "Sustainable Hydrogen Production", *Science*, Vol. 305, No. 5686, pp. 972–974, 2004.

8. Trimm, D., "Minimisation of Carbon Monoxide in a Hydrogen Stream for Fuel Cell Application", *Applied Catalysis A: General*, Vol. 296, No. 1, pp. 1 – 11, 2005.

9. Hinrichsen, K.-O., K. Kochloefl, and M. Muhler, *Water Gas Shift and COS Removal*, Wiley-VCH Verlag GmbH & Co. KGaA, 2008.

10. Ladebeck, J. R. and J. P. Wagner, *Catalyst Development for Water Gas Shift*, John Wiley & Sons, Ltd, Chichester, 2010.

11. Giroux, T., S. Hwang, Y. Liu, W. Ruettinger, and L. Shore, "Monolithic Structures as Alternatives to Particulate Catalysts for the Reforming of Hydrocarbons for Hydrogen Generation", *Applied Catalysis B: Environmental*, Vol. 56, No. 1–2, pp. 95 – 110, 2005.

12. Newsome, D. S., "The Water-Gas Shift Reaction", *Catalysis Reviews*, Vol. 21, No. 2, pp. 275–318, 1980.

13. Soria, M., P. Pérez, S. Carabineiro, F. Maldonado-Hódar, A. Mendes, and L. M. Madeira, "Effect of the Preparation Method on the Catalytic Activity and Stability of Au/Fe2O3 Catalysts in the Low-Temperature Water-Gas Shift Reaction", *Applied Catalysis A: General*, Vol. 470, pp. 45 – 55, 2014.

14. Grenoble, D., M. Estadt, and D. Ollis, "The Chemistry and Catalysis of the Water Gas Shift Reaction: 1. The Kinetics over Supported Metal Catalysts", *Journal of Catalysis*, Vol. 67, No. 1, pp. 90 – 102, 1981.

15. Gorte, R. and S. Zhao, "Studies of the Water-Gas-Shift Reaction with Ceria-Supported Precious Metals", *Catalysis Today*, Vol. 104, No. 1, pp. 18 – 24, 2005.

16. Ratnasamy, C. and J. P. Wagner, "Water Gas Shift Catalysis", *Catalysis Reviews*, Vol. 51, No. 3, pp. 325–440, 2009.

17. Hilaire, S., X. Wang, T. Luo, R. Gorte, and J. Wagner, "A Comparative Study of Water-Gas-Shift Reaction over Ceria Supported Metallic Catalysts", *Applied Catalysis A: General*, Vol. 215, No. 1–2, pp. 271 – 278, 2001.

18. Wang, X., R. Gorte, and J. Wagner, "Deactivation Mechanisms for Pd/Ceria during the Water–Gas-Shift Reaction", *Journal of Catalysis*, Vol. 212, No. 2, pp. 225 – 230, 2002.

19. Zalc, J., V. Sokolovskii, and D. Löffler, "Are Noble Metal-Based Water Gas Shift Catalysts Practical for Automotive Fuel Processing?", *Journal of Catalysis*, Vol. 206, No. 1, pp. 169 – 171, 2002.

20. González, I., R. Navarro, M. Álvarez Galván, F. Rosa, and J. Fierro, "Performance Enhancement in the Water Gas Shift Reaction of Platinum Deposited over a Cerium-Modified TiO2 Support", *Catalysis Communications*, Vol. 9, No. 8, pp. 1759 – 1765, 2008.

21. Sato, Y., K. Terada, Y. Soma, T. Miyao, and S. Naito, "Marked Addition Effect of Re Upon the Water Gas Shift Reaction over TiO2 Supported Pt, Pd and Ir Catalysts", *Catalysis Communications*, Vol. 7, No. 2, pp. 91 – 95, 2006.

22. Thinon, O., F. Diehl, P. Avenier, and Y. Schuurman, "Screening of Bifunctional Water-Gas Shift Catalysts", *Catalysis Today*, Vol. 137, No. 1, pp. 29 – 35, 2008.

23. Kim, Y. T., E. D. Park, H. C. Lee, D. Lee, and K. H. Lee, "Water-Gas Shift Reaction over Supported Pt-CeOx Catalysts", *Applied Catalysis B: Environmental*, Vol. 90, No. 1–2, pp. 45 – 54, 2009.

24. Panagiotopoulou, P. and D. I. Kondarides, "Effect of the Nature of the Support on the Catalytic Performance of Noble Metal Catalysts for the Water-Gas Shift Reaction", *Catalysis Today*, Vol. 112, No. 1–4, pp. 49 – 52, 2006.

25. Boisen, A., T. Janssens, N. Schumacher, I. Chorkendorff, and S. Dahl, "Support Effects and Catalytic Trends for Water Gas Shift Activity of Transition Metals", *Journal of Molecular Catalysis A: Chemical*, Vol. 315, No. 2, pp. 163 – 170, 2010.

26. Lei, Y., N. Cant, and D. Trimm, "Activity Patterns for the Water Gas Shift Reac-

tion Over Supported Precious Metal Catalysts"", *Catalysis Letters*, Vol. 103, No. 1-2, pp. 133–136, 2005.

27. Haruta, M., S. Tsubota, T. Kobayashi, H. Kageyama, M. Genet, and B. Delmon, "Low-Temperature Oxidation of {CO} over Gold Supported on TiO2, a-Fe2O3, and Co3O4", *Journal of Catalysis*, Vol. 144, No. 1, pp. 175 – 192, 1993.

28. Smith, R. J. B., M. Loganathan, and M. Shantha, "A Review of the Water Gas Shift Reaction Kinetics", *International Journal of Chemical Reactor Engineering*, Vol. 8, No. 1, 2010.

29. Zhou, H.-C., J. R. Long, and O. M. Yaghi, "Introduction to Metal-Organic Frameworks", *Chemical Reviews*, Vol. 112, No. 2, pp. 673–674, 2012.

30. Rowsell, J. L. and O. M. Yaghi, "Metal-Organic Frameworks: A New Class of Porous Materials", *Microporous and Mesoporous Materials*, Vol. 73, No. 1-2, pp. 3 – 14, 2004.

31. Silva, C. G., A. Corma, and H. Garcia, "Metal-Organic frameworks as Semiconductors", *Journal of Materials Chemistry*, Vol. 20, pp. 3141–3156, 2010.

32. Kuppler, R. J., D. J. Timmons, Q.-R. Fang, J.-R. Li, T. A. Makal, M. D. Young, D. Yuan, D. Zhao, W. Zhuang, and H.-C. Zhou, "Potential Applications of Metal-Organic Frameworks", *Coordination Chemistry Reviews*, Vol. 253, No. 23–24, pp. 3042 – 3066, 2009.

33. Bhatia, S. K. and A. L. Myers, "Optimum Conditions for Adsorptive Storage", *Langmuir*, Vol. 22, No. 4, pp. 1688–1700, 2006.

34. Sun, Y. Y., Y.-H. Kim, and S. B. Zhang, "Effect of Spin State on the Dihydrogen Binding Strength to Transition Metal Centers in Metal-Organic Frameworks", *Journal of the American Chemical Society*, Vol. 129, No. 42, pp. 12606–12607, 2007.

35. Zhou, W., H. Wu, and T. Yildirim, "Enhanced H2 Adsorption in Isostructural Metal-Organic Frameworks with Open Metal Sites: Strong Dependence of the Binding Strength on Metal Ions", *Journal of the American Chemical Society*, Vol. 130, No. 46, pp. 15268–15269, 2008.

36. Suh, M. P., H. J. Park, T. K. Prasad, and D.-W. Lim, "Hydrogen Storage in Metal-Organic Frameworks", *Chemical Reviews*, Vol. 112, No. 2, pp. 782–835, 2012.

37. Ma, S., D. Sun, J. M. Simmons, C. D. Collier, D. Yuan, and H.-C. Zhou, "Metal-Organic Framework from an Anthracene Derivative Containing Nanoscopic Cages Exhibiting High Methane Uptake", *Journal of the American Chemical Society*, Vol. 130, No. 3, pp. 1012–1016, 2008.

38. Sumida, K., D. L. Rogow, J. A. Mason, T. M. McDonald, E. D. Bloch, Z. R. Herm, T.-H. Bae, and J. R. Long, "Carbon Dioxide Capture in Metal-Organic Frameworks", *Chemical Reviews*, Vol. 112, No. 2, pp. 724–781, 2012.

39. Hamon, L., C. Serre, T. Devic, T. Loiseau, F. Millange, G. Férey, and G. D. Weireld, "Comparative Study of Hydrogen Sulfide Adsorption in the MIL-53(Al, Cr, Fe), MIL-47(V), MIL-100(Cr), and MIL-101(Cr) Metal−Organic Frameworks at Room Temperature", *Journal of the American Chemical Society*, Vol. 131, No. 25, pp. 8775–8777, 2009.

40. Li, J.-R., R. J. Kuppler, and H.-C. Zhou, "Selective Gas Adsorption and Separation in Metal-Organic Frameworks", *Chemical Society Reviews*, Vol. 38, pp. 1477–1504, 2009.

41. Keskin, S. and D. S. Sholl, "Screening Metal-Organic Framework Materials for Membrane-based Methane/Carbon Dioxide Separations", *The Journal of Physical Chemistry C*, Vol. 111, No. 38, pp. 14055–14059, 2007.

42. Czaja, A. U., N. Trukhan, and U. Muller, "Industrial Applications of Metal-Organic Frameworks", *Chemical Society Reviews*, Vol. 38, pp. 1284–1293, 2009.

43. Küsgens, P., M. Rose, I. Senkovska, H. Fröde, A. Henschel, S. Siegle, and S. Kaskel, "Characterization of Metal-Organic Frameworks by Water Adsorption", *Microporous and Mesoporous Materials*, Vol. 120, No. 3, pp. 325 – 330, 2009.

44. Low, J. J., A. I. Benin, P. Jakubczak, J. F. Abrahamian, S. A. Faheem, and R. R. Willis, "Virtual High Throughput Screening Confirmed Experimentally: Porous Coordination Polymer Hydration", *Journal of the American Chemical Society*, Vol. 131, No. 43, pp. 15834–15842, 2009.

45. Do, X.-D., V.-T. Hoang, and S. Kaliaguine, "MIL-53(Al) Mesostructured Metal-Organic Frameworks", *Microporous and Mesoporous Materials*, Vol. 141, No. 1?3, pp. 135 – 139, 2011.

46. Huang, Y., Z. Zheng, T. Liu, J. Lu, Z. Lin, H. Li, and R. Cao, "Palladium Nanoparticles Supported on Amino Functionalized Metal-Organic Frameworks as Highly Active Catalysts for the Suzuki-Miyaura Cross-Coupling Reaction", *Catalysis Communications*, Vol. 14, No. 1, pp. 27 – 31, 2011.

47. Walker, A. M., B. Civalleri, B. Slater, C. Mellot-Draznieks, F. Cora, C. M. Zicovich-Wilson, G. Roman-Perez, J. M. Soler, and J. D. Gale, "Flexibility in a Metal-Organic Framework Material Controlled by Weak Dispersion Forces: The Bistability of MIL-53(Al)", *Angewandte Chemie International Edition*, Vol. 49, No. 41, pp. 7501–7503, 2010.

48. Boutin, A., F.-X. Coudert, M.-A. Springuel-Huet, A. V. Neimark, G. Ferey, and A. H. Fuchs, "The Behavior of Flexible MIL-53(Al) upon CH4 and CO2 Adsorption", *The Journal of Physical Chemistry C*, Vol. 114, No. 50, pp. 22237–22244, 2010.

49. Boutin, A., M.-A. Springuel-Huet, A. Nossov, A. Gedeon, T. Loiseau, C. Volkringer, G. Ferey, F.-X. Coudert, and A. Fuchs, "Breathing Transitions in MIL-53(Al) Metal-Organic Framework Upon Xenon Adsorption", *Angewandte*

Chemie International Edition, Vol. 48, No. 44, pp. 8314–8317, 2009.

50. Ishida, T., M. Nagaoka, T. Akita, and M. Haruta, "Deposition of Gold Clusters on Porous Coordination Polymers by Solid Grinding and Their Catalytic Activity in Aerobic Oxidation of Alcohols", *Chemistry - A European Journal*, Vol. 14, No. 28, pp. 8456–8460, 2008.

51. Park, K. S., Z. Ni, A. P. Côté, J. Y. Choi, R. Huang, F. J. Uribe-Romo, H. K. Chae, M. O-Keeffe, and O. M. Yaghi, "Exceptional Chemical and Thermal Stability of Zeolitic Imidazolate Frameworks", *Proceedings of the National Academy of Sciences*, Vol. 103, No. 27, pp. 10186–10191, 2006.

52. Hermes, S., F. Schroder, S. Amirjalayer, R. Schmid, and R. A. Fischer, "Loading of Porous Metal-Organic Open Frameworks with Organometallic CVD Precursors: Inclusion Compounds of the Type [LnM]a@MOF-5", *Journal of Materials Chemistry*, Vol. 16, pp. 2464–2472, 2006.

53. Jiang, H.-L., B. Liu, T. Akita, M. Haruta, H. Sakurai, and Q. Xu, "Au@ZIF-8: CO Oxidation over Gold Nanoparticles Deposited to Metal-Organic Framework", *Journal of the American Chemical Society*, Vol. 131, No. 32, pp. 11302–11303, 2009.

54. Karakaya, M., *Experimental and Quantitative Analysis of Multiphase Catalytic Reactions under Microfluidic Flow Conditions and Geometries*, Ph.D. Thesis, Bogazici University, 2012.

55. Ertem, O., *Parametric Investigation of Water Gas Shift Over Pd Based Catalysts*, M.S. Thesis, Bogazici University, 2014.